Journal of Materials Chemistry

www.rsc.org/materials

Volume 19 | Number 2 | 14 January 2009 | Pages 173–312

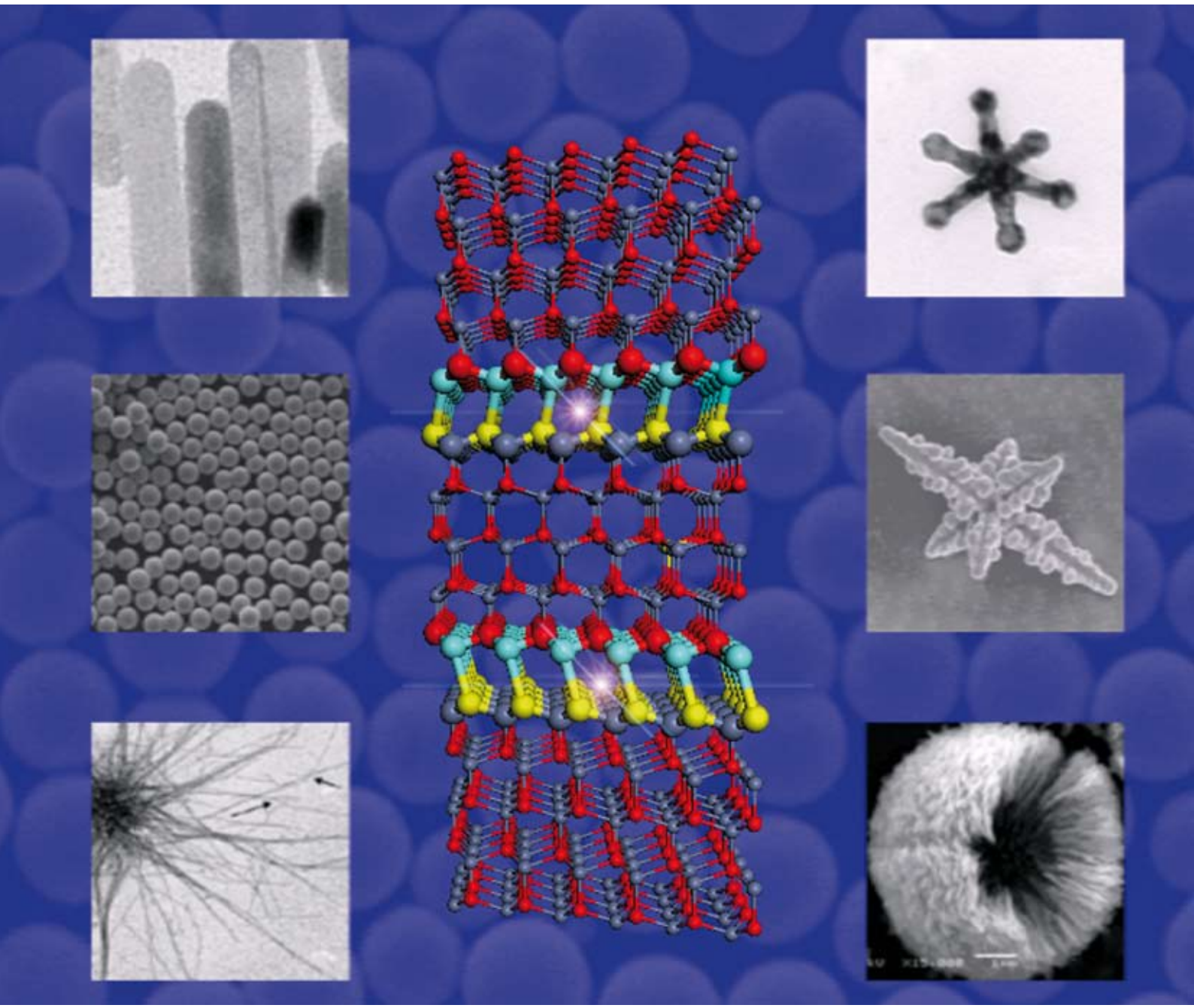

ISSN 0959-9428

RSC Publishing

Recent advances in oriented attachment growth and synthesis of functional materials: concept, evidence, mechanism, and future

Qiao Zhang, Shu-Juan Liu and Shu-Hong Yu*

Received 7th May 2008, Accepted 17th September 2008
First published as an Advance Article on the web 18th November 2008
DOI: 10.1039/b807760f

The latest advances in oriented attachment controlled morphosynthesis and crystal growth of various technically important inorganic materials have been reviewed with the focus on how to generate inorganic micro-/nanostructured materials based on the so-called oriented attachment mechanism. The overview about the basic crystallization principles nowadays falls into two types, i.e., one is the classical crystal growth mode, which is *via* atom-by-atom additions to an existing nucleus or dissolution of unstable phases and reprecipitation of more stable phases, and the other occurs through particle based aggregation modes involving the process of mesoscopic transformation. The systematic analysis of the particle based aggregation mechanism of oriented attachment in controllable synthesis of functional inorganic materials will be described in particular. Several fashions of attachment are undertaken in the already explored reaction systems, with nanoparticles or nanoribbons as primary building units to form 1D, 2D or 3D structures, and heterostructures. The mechanism of oriented attachment could happen in systems with addition of organic additives or without, demonstrating that organic additives are not the essential factor for this kind of growth mode, which shed new light to intensive understanding of this particular phenomenon. With organic additives, i.e., reactions in organic solvents or in aqueous solution, oriented attachment events can occur too. Current developments in oriented attachment, including the basic principles and potentials with specific examples, indubitably reinforce the understanding of detailed interaction mechanisms between inorganic nanoparticles and their subsequent high order self-assembly mechanism, which are definitely promising for rationally designing various kinds of inorganic materials with ideal hierarchy, controllable length scale, and structures in solution-based systems.

1. Introduction

In the past couple of decades, a new field of materials chemistry and physics that emphasizes the rational synthesis and study of nanoscale materials has emerged. Intensive interest in nanomaterials stems from the fact that new properties are acquired at

Division of Nanomaterials and Chemistry, Hefei National Laboratory for Physical Sciences at Microscale, School of Chemistry and Materials, University of Science and Technology of China, Hefei, 230026, P. R. China. E-mail: shyu@ustc.edu.cn; Fax: +0086 551 3603040

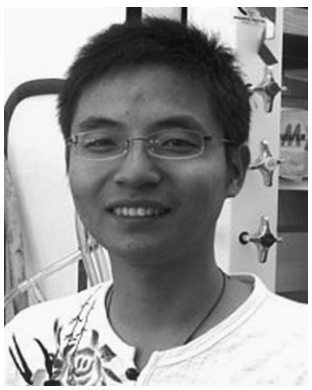

Qiao Zhang

Qiao Zhang received his B.S. degree in Chemistry from University of Science and Technology of China in 2004 and his M.S. degree in Chemistry from University of Science and Technology of China in 2007 under the supervision of Prof. Shu-Hong Yu. He is currently a Ph.D. student in University of California, Riverside. He is especially interested in the fabrication, functionalization and application of nanostructured materials, as well as understanding the fundamental mechanism of formation and properties of nanostructures.

Shu-Juan Liu

Shu-Juan Liu received her B.Sc. in chemistry at Hebei University in 2004. During that time she joined the group of Professor Shi-Wen Ding to work on the research of photocatalytic chemistry. In 2003, she won the second award of the 8th session of "Challenge Cup" national competition of Chinese college students. From 2004 until now her research has been concentrated on the synthesis of functional nanomaterials under the supervision of Prof. Shu-Hong Yu as a Ph.D. candidate in the Department of Chemistry, University of Science and Technology of China.

this length scale and, equally important, that these properties change with their sizes or shapes.[1] Therefore, tailoring the shapes, sizes and properties of nanostructures is one of the major challenges that must be achieved from the viewpoint of applications in nanotechnology. In the past, controlled preparation of nanocrystals with specific sizes and shape has been extensively investigated in studies involving the synthesis of nanoparticles[2–11] and searching for suitable methods for growing anisotropic crystals such as nanowires,[12,13] nanoribbons and nanorods,[14–16] and others.[17–19] However, this is still a very active field strongly motivated by the preparation of nanostructures with tailored morphologies and thus tailored properties using nanoparticles as building blocks.

Solution-based procedures for the preparation of nanostructures (a "bottom-up" approach) are considered very promising because of their potential to allow for precise control over the morphology and sizes of nanoparticles and thus tune their properties. Although crystallization from a solution is such a familiar process that it is likely thought to be fully understood, many key problems are still unsolved in spite of a large amount of research on it.[20]

As accepted for about 100 years, the "Ostwald ripening process" is usually used to explain how a crystal comes into being.[21] For example, many efforts have been focused on anisotropic growth in various systems in which particle coarsening can be well explained by the Ostwald ripening mechanism,[22–25] such as ZnO,[26,27] and TiO_2.[27,28] These systems are characterized by significant solubility of the crystals in the liquid medium, which allows for surface diffusion and generally results in spherical particles. However, intense research on coarsening behavior and morphology evolution of nanomaterials shows that the Ostwald ripening mechanism cannot explain all phenomena well. For instance, some studies have demonstrated the possibility of fostering anisotropic growth in these systems by maintaining the solute concentration higher than the equilibrium concentration.[6,15,29] Peng *et al.*[7] also stated that the supersaturation state in solution prevents the smaller particles from being dissolved, and growth occurs by precipitation of dissolved ions in high-energy facets instead of coarsening.

On the other hand, Penn and Banfield presented a new crystal growth mechanism, the so-called "oriented attachment" mechanism, in which secondary mono-crystalline particles can be obtained through attachments of primary particles in an irreversible and highly oriented fashion.[30–34] This process seems very promising as a route for the preparation of complex-shaped nanostructures using primary nanoparticles themselves as building blocks, which has been reported previously in the role of "oriented attachment" in anisotropic growth of nanocrystals,[12,30–36] such as α-Fe_2O_3,[37,38] Fe_3O_4,[39] PAu,[40] hydroxyapatite ($Ca_{10}(PO_4)_6(OH)_2$),[41] CdTe, PbSe,[42] SnO_2,[16,43] TiO_2,[44,45] and ZnS.[46,47] In these systems, the bigger particles are grown from small primary nanoparticles through an oriented attachment mechanism, in which the adjacent nanoparticles are self-assembled by sharing a common crystallographic orientation and docking of these particles at a planar interface. The driving force for this spontaneous oriented attachment is that the elimination of the pairs of high energy surfaces will lead to a substantial reduction in the surface free energy from the thermodynamic viewpoint.[33,48] In this Feature Article, recent advances in this special emerging field will be reviewed. We start with a discussion of basic theories and general views in crystal growth in Section 2. Then, in Section 3, concepts and development of oriented attachment mechanism will be discussed, and some selected examples will be presented to highlight the importance and versatility of this new crystal growth mechanism for materials science on the way to the development of new strategies for shaping crystals and morphogenesis, and hence, their related properties.

2. Crystal growth modes and aggregation modes

2.1 Classical crystal growth mode

Classically, growth of crystals has been thought to occur by atom-by-atom or monomer-by-monomer addition to an inorganic or organic template or by dissolution of unstable phases (small particles or metastable polymorphs) and reprecipitation of the more stable phase.[49] Thus, the chemical growth of bulk or nanometer-sized materials inevitably involves the process of precipitation of a solid phase from solution. A good understanding of the process and parameters controlling the precipitation helps to improve the engineering of the growth of nanoparticles to the desired size and shape. For a particular solvent, there is a certain solubility for a solute, whereby addition

Shu-Hong Yu

Shu-Hong Yu was born in 1967. He received his PhD in Inorganic Chemistry in 1998 from University of Science and Technology of China under the supervision of Prof. Yi-Tai Qian. From 1999 to 2001, he joined Prof. Masahiro Yoshimura's Lab in Materials and Structures Laboratory, Tokyo Institute of Technology, as a JSPS Research Fellow. From 2001 to 2002, he was as an Alexander von Humboldt Research Fellow in the Max Planck Institute of Colloids and Interfaces, Potsdam, Germany, working with PD Dr habil. Helmut Cölfen and Prof. Dr Markus Antonietti. He was appointed as a full professor in 2002 and the Cheung Kong Professorship in 2006 in the Department of Chemistry, University of Science and Technology of China (USTC). Currently, he is leading the Division of Nanomaterials & Chemistry, Hefei National Laboratory for Physical Sciences at Microscale (HFNL). His research interests include bio-inspired synthesis and self-assembly of new nanostructured materials and hybrids, carbon related materials, and their related properties. He has authored and co-authored more than 150 refereed journal publications, and 8 invited book chapters. He serves as an associate editor for international journal Materials Research Bulletin*, and is a board member of journal* Current Nanoscience*.*

of any excess solute will result in precipitation and formation of nanocrystals. Thus, in the case of nanoparticle formation, for nucleation to occur, the solution must be supersaturated either by directly dissolving the solute at higher temperature and then cooling to low temperatures, or by adding the necessary reactants to produce a supersaturated solution during the reaction.[6,50] The precipitation process then basically consists of a nucleation step followed by particle growth stages.[51,52]

Generally, there are three kinds of nucleation processes: homogeneous nucleation, heterogeneous nucleation, and secondary nucleation. We consider the simplest case of homogeneous nucleation, which occurs in the absence of a solid interface by combining solute molecules to produce nuclei. Homogeneous nucleation happens due to the driving force of the thermodynamics because the supersaturated solution is not stable in energy. The overall free energy change, ΔG, is the sum of the free energy due to the formation of a new volume and the free energy due to the new surface created. For spherical particles

$$\Delta G = -\frac{4}{V}\pi r^3 k_B T \ln(S) + 4\pi r^2 \gamma \quad (1)$$

where V is the molecular volume of the precipitated species, r is the radius of the nuclei, k_B is the Boltzmann constant, S is the saturation ratio, and γ is the surface free energy per unit surface area. When $S > 1$, ΔG has a positive maximum at a critical size, r^* (Fig. 1).

$$r^* = \frac{2V\gamma}{3k_B T \ln(S)} \quad (2)$$

This maximum free energy is the activation energy for nucleation. Nuclei larger than the critical size will further decrease their free energy for growth and form stable nuclei that grow to form particles. The critical nuclei size r^* can be obtained by setting $d\Delta G/dr = 0$.

For a given value of S, all particles with $r > r^*$ will grow and all particles with $r < r^*$ will dissolve. From the above equation, it follows that the higher the saturation ratio S, the smaller the critical nuclei size r^* is. In addition, the other nucleation processes are also presented by Markov based on a thermodynamics approach.[53]

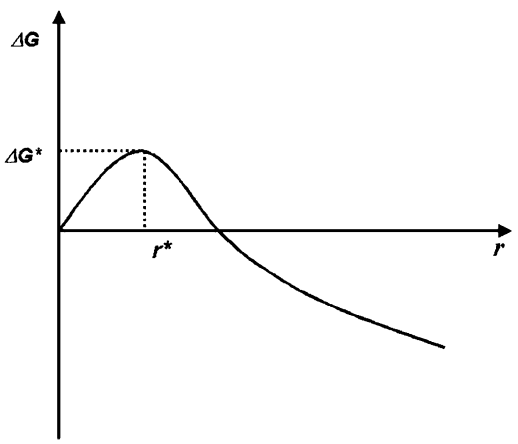

Fig. 1 Illustration of the overall free energy ΔG as a function of the growth particle size r. From ref. 1. Copyright © 2005 American Chemical Society.

When the concentration of growth species reduces below the minimum concentration for nucleation, nucleation stops, whereas the growth continues until the equilibrium concentration of the precipitated species is reached.[54] Uniformity of the size distribution is achieved through a short nucleation period that generates all of the particles obtained at the end of the reaction followed by a self-sharpening growth process. At this stage, kinetic control and focusing of size occurs: the smaller particles grow more rapidly than the larger ones because the free energy driving force is larger for smaller particles than for larger ones if the particles are slightly larger than the critical size. By taking advantage of this key feature, nearly monodisperse size distribution can be obtained at this stage by either stopping the reaction (nucleation and growth) quickly or by supplying a reactant source to keep a saturated condition during the reaction.

On the other hand, when the reactants are depleted due to particle growth, Ostwald ripening or defocusing will occur, where the larger particles continue to grow, and the smaller ones get smaller and finally dissolve. Because the saturation ratio (S) decreases now and the corresponding critical nuclei size (r^*) increases according to eq (2), any particles smaller than this new critical size will dissolve. If the reaction is quickly stopped at this stage, the particles will have a broad size distribution, which is featured by a distribution centering two size regimes, a bigger one and a smaller one, and the critical size now at this saturation is in between. Once the reaction (mainly the growth of the particles) goes into this stage, it is difficult to get monodisperse particles unless the reaction is extended to long enough time to completely deplete the supersaturation and the smaller nuclei. In the latter case, the size of the particles gets relatively large and can extend into the micrometer size regime. During an actual experiment, when there is no continuous supply of the reactants, the saturation ratio continues to decrease and the critical nuclei size continues to increase. To get a short burst of nucleation, a high saturation ratio (S) is required.

In the simplest form of classical crystal growth theory,[55] atoms/molecules continually bond and dissolve, attach occasionally to the surface of a large crystal seed in one of many ways, and then perhaps join together as part of a growing structure of spiraling mounds, spreading layers, and small islands. Molecules land on the surface of a growing seed and become weakly adsorbed. They may join together to form small, two-dimensional islands and spread outward in a layer (called a "step") one molecule thick, with other islands forming and growing on top. In this dynamic growth process, molecules continually absorb onto and dissolve from islands.

2.2 Aggregation modes

In addition to the ion-mediated classical crystal growth by atom/molecular addition where soluble species deposit on the solid surface, particles can grow by aggregation with other particles involving a mesoscopic transformation process.[56] The rate of particle growth by aggregation is much larger than that by atom/molecular addition. After the particles grow to a stable size, they will grow by combining with smaller unstable nuclei rather than by collisions with other stable particles. The main pathways of aggregation-based crystallization are illustrated in Fig. 2.[57] The

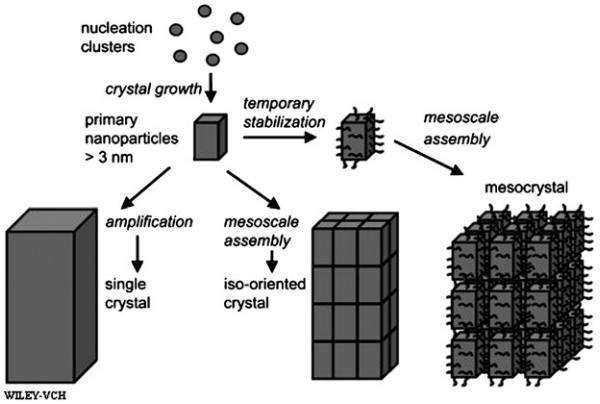

Fig. 2 Schematic representation of classical and aggregation-based crystallization. (Left) Classical crystallization pathway (a), (centre) oriented attachment of primary nanoparticles forming an iso-oriented crystal upon fusing (path (b)), (right) mesocrystal formation *via* self-assembly of primary nanoparticles covered with organics (path (c)). From ref. 57. Copyright © 2005 Wiley-VCH.

classical crystal growth model is described by path (a). Path (b) involves the arrangement of primary nanoparticles into an iso-oriented crystal *via* oriented attachment, which can form a single crystal upon fusion of the nanoparticles. If the nanoparticles are coated by some organic components, they can form a mesocrystal *via* mesoscale assembly (path (c)), possibly followed by fusion to an iso-oriented crystal and finally to a single crystal.[58–61] To the best of our knowledge, more and more mesocrystals built from three-dimensional (3D) and well-aligned crystals while exhibiting scattering properties similar to a single crystal have been observed, such as CdS,[62] $CoC_2O_4 \cdot 2H_2O$,[63] $CaCO_3$,[64–72] $BaCO_3$,[73] D,L-alanine,[57,74] $CoPt_3$,[75] ZnO-PVP nanocomposites,[76] even Au[77] and Ag.[78]

Nanoparticles are small and are not thermodynamically stable for crystal growth kinetically. To finally produce stable nanoparticles, these nanoparticles must be arrested during the reaction either by adding surface protecting reagents, such as organic ligands or inorganic capping materials, or by placing them in an inert environment such as an inorganic matrix or polymer. The nanocrystal (NC) dispersions are stable if the interaction between the capping groups and the solvent is favorable, providing an energetic barrier to counteract the van der Waals and magnetic attractions (magnetic materials) between nanoparticles.[79] To help arrest these nanoparticles, different solvents are also used to change the solubility or the reaction rate.[50,52]

Aggregation-based crystallization offers some peculiar advantages with respect to crystal morphogenesis such as the near independence of solubility products and indifference to pH and osmotic pressure. These features are particularly relevant in biological systems and accordingly the study of non-classical crystallization processes is documented for biomineralization. Recently, the investigation of the role of amorphous precursor particles has attracted a lot of attention,[56,80–86] rather than the investigation of oriented attachment or mesocrystal formation.[87–89] However, a look into recent literature clearly reveals that these new crystallization routes will also play a vital role in materials science, for example, in the synthesis of advanced functional materials.

3. Oriented attachment growth: new mechanism

Traditional solution synthesis methods have been widely used for the controlled synthesis of various colloidal nanoparticles.[95,96] Classically, crystal coarsening has been described in terms of growth of large particles at the expense of smaller particles.[97] The driving force for this so-called Ostwald ripening process is the surface energy reduction. In this process, the formation of tiny crystalline nuclei in a supersaturated medium occurs first and then is followed by crystal growth, in which the larger particles will grow at the cost of the small ones due to the energy difference between large particles and the smaller particles of a higher solubility based on the Gibbs–Thompson law.[98]

While in these systems the bigger particles are grown from small primary nanoparticles through an oriented attachment mechanism, the adjacent nanoparticles are self-assembled by sharing a common crystallographic orientation and docking of these particles at a planar interface. The driving force for this spontaneous oriented attachment is that the elimination of the pairs of high energy surfaces will lead to a substantial reduction in the surface free energy from the thermodynamic viewpoint.

Averback et al. identified a similar spontaneous self-assembly process which they called "contact epitaxy" during their study of the deposition of Ag nanoparticles onto Cu substrates.[99,100] The initial randomly oriented Ag nanocrystals can align epitaxially with the substrate, which was explained as the rotation of the nanoparticles within the aggregates driven by short-range interactions between adjacent surfaces.[99] Increasing evidence in several systems has been observed for either directed particle aggregation or undirected particle aggregation. This kind of growth mode could lead to the formation of faceted particles or anisotropic growth if it occurs near equilibrium and there is sufficient difference in the surface energies of different crystallographic faces. It is possible to form perfect highly anisotropic crystals, which clearly show the growth *via* oriented attachment as impressively evidenced for TiO_2.[32]

In 1999, Penn and Banfield[32] reported that in the case of hydrothermally coarsened anatase TiO_2, the nanoparticles assemble into single crystalline structures composed of several primary crystallites (Fig. 3). The crystallographic orientation of the particles with respect to each other is determined by the minimization of the highest energy surfaces. When two nanoparticles approach each other closely enough, they are mutually attracted by van der Waals forces. However, due to their thermal energy, they can still rearrange to find the low-energy configuration represented by a coherent particle–particle interface.[33,101–103] There are a few studies emerging recently, which deal with the kinetics of the oriented aggregation by Penn,[101] Leite et al.,[102] and

Fig. 3 (a) TEM micrograph of hydrothermally coarsened anatase particles forming a chain-like nanostructure, (b) HRTEM of a part of such an assembly proving the single crystalline nature. From ref. 32. Copyright © 1999 Elsevier Sciences.

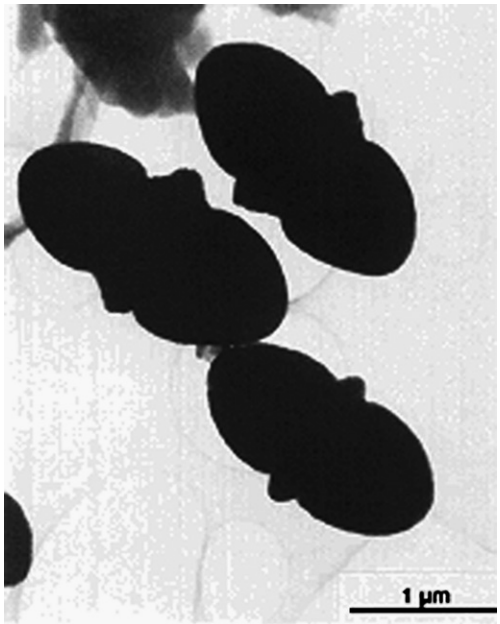

Fig. 4 TEM image showing α-Fe_2O_3 double-ellipsoids produced by aging a solution (0.018 M $FeCl_3$, 0.05 M HCl) at 100 °C for one week. From ref. 37. Copyright © 1993 Elsevier Sciences.

the mathematical models for crystal growth through aggregation of metastable precursor nanoparticles by Tsapatsis et al.[103]

An early interesting finding by Bailey et al.[37] shows that a rather complex morphology of α-Fe_2O_3 double-ellipsoids (Fig. 4) can be easily obtained through aging a solution containing β-FeOOH rods at 100 °C for one week which was obtained by a hydrolysis reaction of $FeCl_3$ in HCl solution. These complex double-ellipsoid structures were clearly developed from the heterogeneous nucleation of hematite on β-FeOOH rods formed in the early stage. The α-Fe_2O_3 (hematite) particles not only grow outward but also use these rods as templates and a collar forms along the rods, leading to the formation of such double-ellipsoid shapes. This example shows that the size and aggregation of the metastable phase can influence the final morphology.

Oriented attachment offers the special advantage of producing defect-free one-dimensional single crystals, which is certainly of interest in materials science. Classical crystallization always causes defect structures in the form of branches when attempting fibre growth by additive adsorption to all crystal faces parallel to the growth axis and thus these faces become blocked from further growth. In contrast, oriented attachment offers the crystallographic fusion of nanoparticles to single crystalline and defect-free fibres, which can be hundreds of micrometers long. This is demonstrated in the example of hydroxyapatite (HAP) fibres (Fig. 5a), whose aggregates of special block copolymers were adsorbed to all faces parallel to the *c*-growth axis.[94]

Although thin and long crystalline HAP fibres were obtained (the single crystalline nature of the fibres could not be shown due to their small diameter of only 2–3 nm), the fibres clearly show occasional branches (Fig. 5a, d). These can be attributed to a noncontinuous polymer layer, so that branching can occur at the non-covered sites on the crystal as result of the ion-based classical growth mechanism. On the other hand, if all crystal

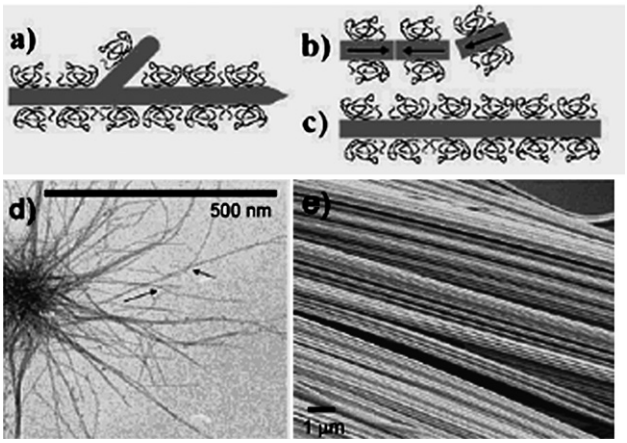

Fig. 5 Classical (a) vs. non-classical crystallization (b, c). (a) Crystallization of hydroxyapatite (HAP) fibres from block copolymer aggregates,[90] where the block copolymers adsorb to all faces parallel to the HAP *c*-growth axis resulting in whisker structures with occasional branches (d, see arrows). (b, c, e) Formation of single crystalline and defect-free $BaSO_4$ (210) oriented fiber bundles by oriented attachment process in experiments described in ref. 91–93. From ref. 94. Copyright © Editorial Universitaria.

faces parallel to one axis of a nanoparticle are already covered by polymers, only two opposite faces remain uncovered and thus become high energy faces. These faces can then fuse together to form a single crystalline fibre without any defects following the mechanism of oriented attachment (Fig. 5b, c). Here, the advantages of the particle-based mechanism compared to the ion-based one become directly obvious.

It has to be pointed that the oriented attachment is not only described for the one-dimensional case, but is also described for two- and three- dimensional cases.[104] In addition, when combined with other synthesis methods, oriented attachment mechanism could also be used to organize hierarchical structures in three dimensions with or without hollow interiors, which has been expatiated in a review by Zeng.[105]

3.1 Oriented attachment growth in the presence of organic additives

The shape of a crystal is determined by the relative specific surface energies associated with the facets of this crystal. At equilibrium, a crystal has to be bounded by facets giving a minimum total surface energy, an argument that is known as the Wulff facets theorem.[106] Confined by this requirement, the shape of a single crystalline nanostructure often reflects the intrinsic symmetry of the corresponding lattice (for most metals, it is a cube rather than a rod).[107–113] The shape of a crystal can also be considered in terms of growth kinetics, by which the fastest growing planes should disappear to leave behind the slowest growing planes as the facets of the product.[114,115] This argument implies that one can control the final shape of a crystal by introducing appropriate organic molecules to change the free energies to alter their growth rates, and hence, in order to control their size, shape and even structure.[116,117] In the past, a range of compounds have been evaluated as capping reagents (or so-called surface-modifiers) to control the shape of colloidal

particles synthesized using solution-phase methods.[118–121] In addition, the use of organic compounds as templates for the generation of inorganic structures and materials has received increasing attention over the last decade.[122–127] Here, we present some selected examples to highlight how the "oriented attachment" model works in the presence of organic additives.

TiO_2. In their early studies on TiO_2, Penn and Banfield[30,31] have found that organic molecules may hinder or modify the oriented attachment process. In the case of TiO_2, organics adsorbed in a crystallographically specific manner can suppress (as in the case of adipic acid, acetic acid, and glycine) or modify the oriented attachment process by preventing contact between the faces on which adsorption has selectively occurred. In previous studies, it is believed that one step in oriented attachment is the surface functionalization of nanoparticles with low molecular weight ligands (the "assembler"), which predetermine the assembly behaviour of the nanoparticles. This idea was applied in the case of titania nanoparticles coated with various multidentate ligands.[14,128] The synthesis was performed with benzyl alcohol[129–131] in the presence of trizma $(HOCH_2)_3CNH_2$, resulting in the formation of a powder composed of surface-functionalized anatase nanocrystals with diameters of about 3 nm. Upon redispersion in water the nanoparticles self-organized into pearl necklace structures with total length of several hundreds of nanometers (Fig. 6a). Interestingly, these nanowire-like arrangements were composed of a continuous string of precisely ordered nanoparticles. High resolution transmission electron microscopy (HRTEM) investigations gave evidence that the nanoparticles assembled along the [001] direction *via* oriented attachment, exhibiting monocrystal-like lattice fringes (Fig. 6b). Experimental data indicate that the anisotropic assembly is a consequence of the water-promoted desorption of the organic ligand selectively from the {001} faces of the crystalline nano-sized building blocks together with dissociative adsorption of water on these crystal faces. Both processes induce the preferred attachment of the titania nanoparticles along the [001] direction. The use of polydentate and charged ligands to functionalize the surface of titania nanoparticles thus provides a versatile tool to control their arrangement on the nanoscale.

Hydroxyapatite. Nancollas and colleagues have mimicked the self-organized microstructure of tooth enamel.[132] They found that at near-physiological pH value, temperature, and ionic strength, amelogenin (Amel) can accelerate hydroxyapatite (HAP) nucleation kinetics, decreasing the induction time in a concentration-dependent manner. Hierarchically organized apatite microstructures can be formed by self-assembly involving nucleated nanocrystallites and Amel oligomers and nanospheres at low supersaturations and protein concentrations in a slow and well-controlled constant composition (CC) system. This CC method allows the capture of an intermediate structure, i.e. the nanorod, following the formation of the critical nuclei at the earliest nucleation stages of calcium phosphate crystallization. The nanorod building blocks formed spontaneously by synergistic interactions between flexible Amel protein assemblies and rigid calcium phosphate nanocrystallites. These intermediate structures further assemble by oriented attachment to form the final hierarchically organized microstructures that are compositionally and morphologically similar to natural enamel (Scheme 1).

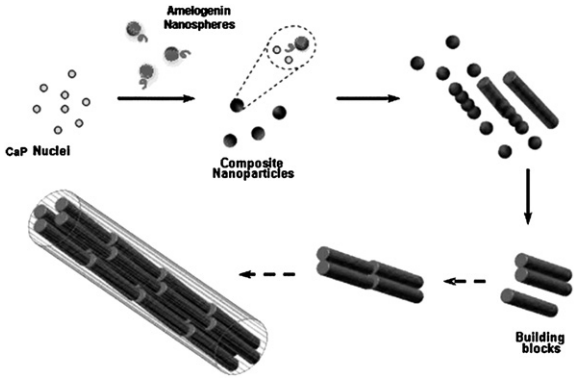

Scheme 1 Mechanism illustration of in vitro hierarchically organized microstructure formation by self-assembly of nucleated apatite nanocrystallite–Amel nanosphere mixtures based on experimental evidence (solid arrows) and theoretical analysis (dotted arrows). From ref. 132. Copyright © 2008 American Chemical Society.

PbSe. A recent report by Cho et al.[42] provided some strong evidence that nearly defect-free PbSe nanowires with different morphologies, such as straight, zigzag, helical, branched, and tapered nanowires as well as nanorings, can be conveniently synthesized by careful adjustment of different organic additives. Their results suggest that PbSe nanocrystals could bind to each other on either {100}, {110}, or {111} faces, depending on the surfactant molecules present in the reaction solution. In addition, the chemical nature of stabilizing agents can significantly affect the surface energy of the different facets of PbSe nanocrystals and nanowires. Addition of long-chain, aliphatic primary amines (*e.g.*, dodecylamine, hexadecylamine (HDA), oleylamine, etc.) to the reaction mixture as cosurfactants induces the formation of octahedral PbSe nanocrystals terminated by eight {111} facets (Fig. 7a). Zigzag nanowires can also be obtained using primary amines by injection at 250 °C and growth at 170 °C (Fig. 7b). When the nanowires are formed with HDA and oleic acid as cosurfactants in the reaction medium of trioctylamine, the formation of single-crystal helical PbSe nanowires has been observed (Fig. 7c). Helical PbSe nanowires can also be prepared by the annealing of straight PbSe nanowires at 180–200 °C in the presence of trioctylamine and oleic acid (Fig. 7d).

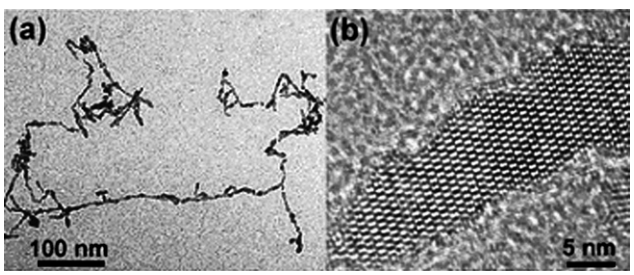

Fig. 6 (a) TEM image of wire-like nanostructures composed of trizma functionalized anatase nanoparticles, (b) HRTEM image of a part of such a nanoparticle assembly. From ref. 14. Copyright © 2004 Wiley-VCH.

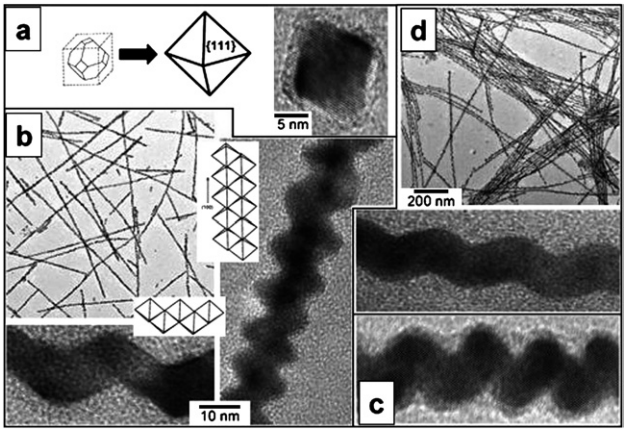

Fig. 7 (a) Octahedral PbSe nanocrystals grown in the presence of HDA and oleic acid. (b) TEM and high-resolution TEM images of PbSe zigzag nanowires grown in the presence of HDA. The cartoons show packing of octahedral building blocks to form the nanowires. (c) HRTEM images of single-crystal helical PbSe nanowire grown in oleic acid/HDA/trioctylamine mixture. (d) Helical nanowires formed upon annealing of straight PbSe nanowires, as shown in (c), in the presence of trioctylamine. From ref. 42. Copyright © 2005 American Chemical Society.

CdSe. Pradhan et al.[133] reported a relatively low temperature (100–180 °C) synthesis route to obtain high-quality and single-crystalline CdSe nanowires using alkylamines, a single type or a mixture of two different types of amines, with different chain lengths and varying the reaction temperature. The diameter of nanowires was controlled and varied in an exceptionally small size regime, between 1.5 and 6 nm, by changing the chain length of the amines. More than that, the chain length of the organic additives can also affect the self-assembly of the nanowires. As shown in Fig. 8, all solid nanowires are single-crystalline with wurtzite crystal structure although they were grown in the typical zinc blende preferred temperatures, between 120 and 180 °C. The long axes of these quantum wires were found to be the *c* axis of the wurtzite structure, which is the same as the quantum rods formed under high temperatures.[134–136] A similar orientation was also observed for the catalyst-promoted growth of CdSe wires in both solution[137] and gas phase.[138] In addition, the experimental results suggest the coexistence of two types of fragments in the pre-wire aggregates, known as "pearl-necklace" or "string-of-pearls" in the literature, which are loosely associated and chemically fused sections.

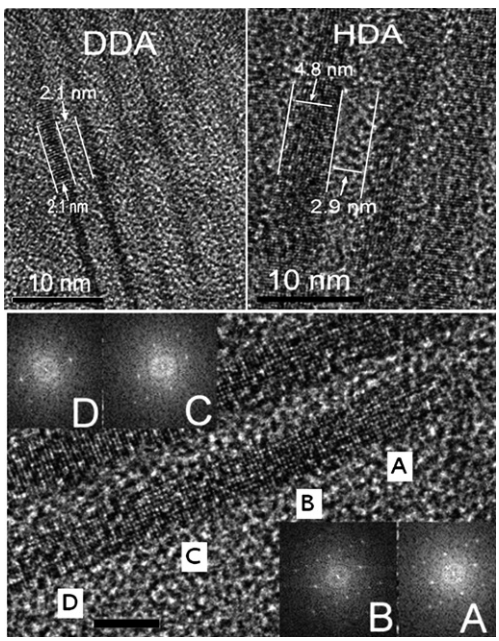

Fig. 8 High-resolution TEM images of CdSe quantum wires. Bottom inserts (A–D) are FFT patterns of the corresponding places marked on the nanowire. These nanowires are formed in a mixture of DDA and HDA. From ref. 133. Copyright © 2006 American Chemical Society.

CdTe. Kotov et al.[12] have demonstrated the formation of luminescent CdTe nanowires *via* crystal dipole-induced self-assembly of CdTe nanoparticles. CdTe nanoparticles were found to spontaneously reorganize into crystalline nanowires upon controlled removal of the protective shell of organic stabilizer, and the diameter of these as-synthesized nanowires was determined by the diameter of the original nanoparticles. The produced nanowires have high aspect ratio, uniformity, and optical activity.

The as-produced nanowires are single-crystalline in structure, albeit with some defects (Fig. 9A and B). Lattice plane spacings calculated from the diffraction patterns are 3.98 Å hkl (100) and 2.29 Å hkl (110) and are typical for hexagonal wurtzite CdTe structures. As shown by vector diagrams in Fig. 9, the

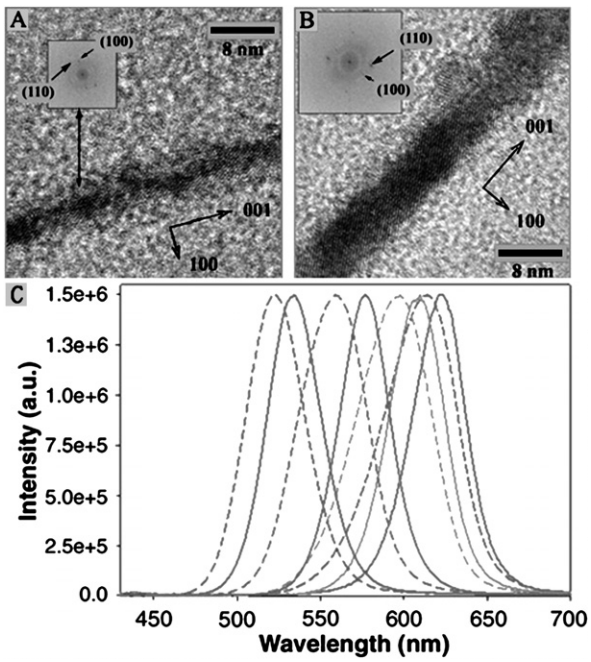

Fig. 9 (A), (B) High-resolution TEM of nanowires made from (A) orange- and (B) red-emitting CdTe quantum dots. The insets show the corresponding diffraction patterns for (001) and (100); vectors of the crystal lattice are indicated by thick arrows. (C) Luminescence spectra of parent CdTe nanoparticles (dashed lines) and resulting nanowires (solid lines) marked by the corresponding luminescence colors. From ref. 12. Copyright © 2006 AAAS.

perpendicular orientation of the (100) planes with respect to the nanowire axis and slanted (110) plane projection indicates that the long axis of the nanowires is parallel to the (001) direction of the wurtzite crystal lattice. This orientation is maintained for all nanowires produced, regardless of the initial particle size. CdTe nanocrystals have the cubic zinc blend structure, and, therefore, the nanowire growth is accompanied by a phase transition. This occurs because the hexagonal lattice is intrinsically anisotropic and has a unique (001) axis. CdTe nanocrystals reorganize their lattice to obtain the match between the symmetry of the crystal and the uniaxial geometry of 1D species. This process is facilitated by the low activation energy of phase transition of CdTe and by the partial removal of the stabilizer coating. Four different CdTe dispersions with luminescence maxima at 520 to 530 (green), 550 to 565 (yellow), 590 to 605 (orange), and 610 to 625 (red) nm were used for the preparation of nanowires (Fig. 9C). As expected, the nanowire growth was accompanied by the red shift of the luminescence peaks of the dispersion, which reached its maximum of 10 to 20 nm in 7 days (Fig. 9). The red shift occurs due to the decrease of confinement in one dimension.

Au. Recently, Ravishankar et al. obtained ultrathin single-crystalline Au nanowires *via* addition of ascorbic acid to a mixture containing gold nanoparticles and aging at room temperature for an extended period.[139] It is demonstrated that the formation of Au wires is due to a preferential removal of the capping agent of amine from the {111} planes of the nanoparticles and then fusion. The difference in amine/gold binding energy on different facets of gold enables preferential removal of the capping agent from one of the facets and promotes formation of anisotropic structures. Actually, the removal of amine from the surface caused by the reaction with ascorbic acid takes place along with the adsorption of amine from the solution phase on the exposed surfaces. Thus, the growth of the wire will depend upon the rate of attachment of the exposed nanoparticles along the {111} surfaces compared to the rate of adsorption of the amines from the solution phase. It has been proposed that when two faceted particles come into contact the alternate convex and concave regions that formed lead to a difference in chemical potential which would result in the smoothing process of the particles by diffusion. Owing to the time of the smoothing process being much shorter than the average time between collisions, the dominant product of the reaction would be wires. Moreover, albeit with a much lower probability the attachment can still take place along one of the other {111} facets, which results in the formation of extended bunches of parallel self-assembled nanowires (Fig. 10). Several steps were reported to go along with the formation of nanowire arrays,: first, particle attachment takes place along a <111> direction that is different from the growth direction of the wire (Fig. 10A); subsequently, growth proceeds along that direction or turn back to the original orientation (Fig. 10B); finally both types of growth take place, leading to the formation of extended arrays of parallel nanowires which contain several tens of parallel segments (Fig. 10C, D).

MnO. Another interesting example of oriented attachment is observed in the synthesis of MnO multipods[140] (Fig. 11). The MnO multipods were achieved *via* a non-hydrolytic sol–gel process in a mixture of $Mn(oleate)_2$, oleic acid and trioctylamine. TEM micrographs show predominantly hexapods (Fig. 11a,b), however 2, 3, 4 or 5 pods (Fig. 11c) were found in the sample, too. The cores of the pods as well as the pods themselves are uniform in size and each arm is terminated by an arrow-like shape. Selected area electron diffraction (SAED) from isolated multipods proved their single-crystalline nature. Considering the cubic rock salt structure of MnO, anisotropic crystal growth is unexpected. To explain this behaviour, a two-step mechanism has been proposed, involving nucleation of truncated octahedra or cubes, followed by oriented attachment of the nanoparticles into the final pod morphology. As a matter of fact, nanoparticles matching the size of the tetrapod building blocks with a truncated octahedral shape were found when decreasing the reaction time. Other examples of the one-dimensional assembly

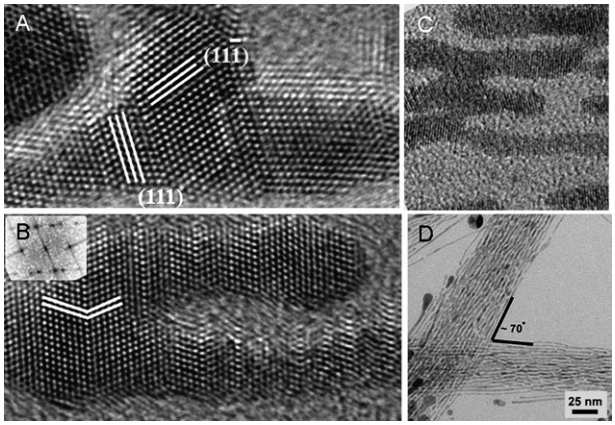

Fig. 10 This shows the early stages of formation of Au nanowire arrays by the oriented-attachment process. In (A) a particle attaches along one of the {111} facets that is different from the growing direction. B) The branched region branches again to form a segment parallel to the original wire. C) The process leading to the formation of parallel arrays. D) Lower-magnification image showing two sets of parallel-wire arrays at an angle of *ca.* 70° where growth has taken place along two different <111> directions. From ref. 139. Copyright © 2007 Wiley-VCH.

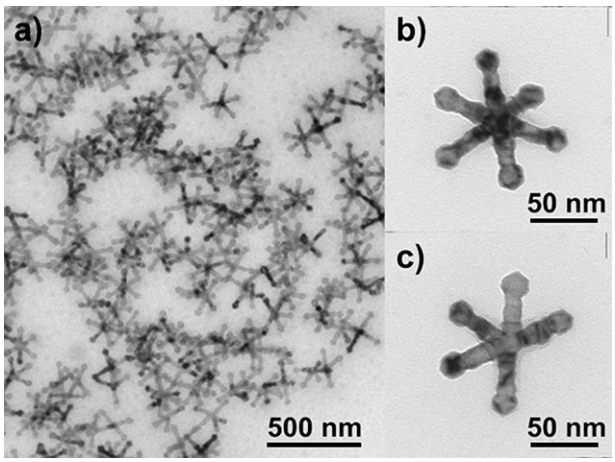

Fig. 11 An overview TEM image of an assembly of MnO multipods (a), a hexapod (b), and a pentapod (c). From ref. 140. Copyright © 2005 American Chemical Society.

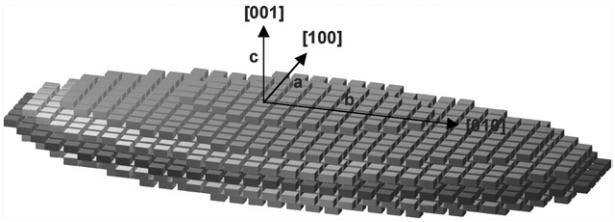

Scheme 2 Schematic illustration of a single-crystalline assembly of cupric oxide built from aggregated nanoparticles. From ref. 142. Copyright © 2005 Wiley-VCH.

of nanoparticles were discussed in a recent review by Tang and Kotov.[141]

CuO. As illustrated in Scheme 2, Han et al. reported a simple synthesis approach to building monocrystalline CuO from nanoparticles at room temperature taking advantage of oriented attachment.[142] They have demonstrated an anisotropic aggregation-based crystal growth process of a few hundred monoclinic CuO nanoparticles into uniform ellipsodial monocrystalline architectures. Stepwise orientation and aggregation of a large number of nanoparticles in three dimensions has been observed, from the formation of primary CuO nanoparticles, to the preferential one-dimensional (1D) orientation of nanoparticles along the (001) direction at an early stage, and, eventually, 3D-oriented aggregation into a monocrystalline structure built from nanoparticles. Selective adsorption of formamide molecules on different crystallographic planes of monoclinic CuO nanoparticles may play an important role in the anisotropic growth of uniform nanoparticle-built monocrystals.

Common surfactants can also be used to adsorb onto nanoparticle surfaces in a reverse microemulsion, resulting in an oriented attachment process, which finally leads to the formation of fibres, as reported for $BaSO_4$ in a reverse microemulsion with AOT.[143,144] Aside from low molar mass ligands, polymers can also be applied to coat nanoparticle surfaces by selective polymer adsorption for subsequent oriented attachment. An example is the formation of $BaSO_4$ or $BaCrO_4$ defect-free fibres of about 30 nm in diameter but up to hundreds of μm in length, which were formed in the presence of polyacrylate or a phosphonated double hydrophilic block copolymer at room temperature in water.[91–93,145–148]

$PbWO_4$. A surfactant-assisted method has been developed to synthesize $PbWO_4$ micro-crystals with special hierarchical structures by taking advantage of the "oriented attachment" mechanism.[149] The cationic surfactant cetyltrimethylammonium bromide (CTAB) is used to synthesize homogeneous dendritic $PbWO_4$ microcrystals, as shown in Fig. 12a,b, which are quite similar to those reported for cubic PbS microstructures.[150,151] Two shorter trunks and a longer one, these three crossed trunks construct the framework in a perfect perpendicular manner. Four branches grow vertically on each trunk in two perpendicular directions, which are similar to the growth directions of the other two trunks, and ordered microrods parallel to each other form the branches. The length of the longer trunk is about 20 μm and that of the two branches is about 9 μm. The ratio of the lengths of the three main trunks is equal to the ratio of the cell

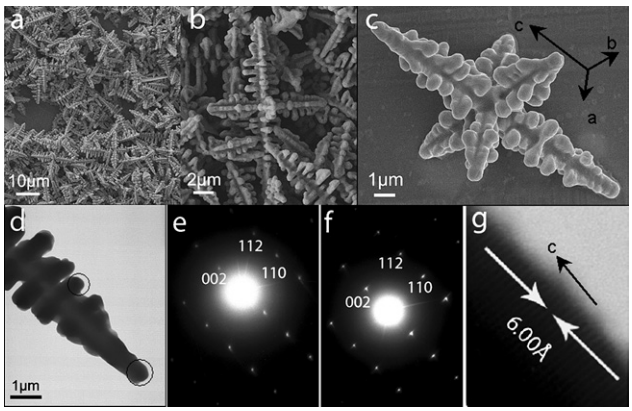

Fig. 12 SEM images, TEM images, and ED patterns of the $PbWO_4$ dendrites obtained after aging at 60 °C for 18 h. a) A general view of the sample; b) a higher magnification SEM image; c) a typical single dendrite; d) a magnified TEM image showing part of the dendrite; e) ED pattern recorded from the branched part marked with circles in (d); f) ED pattern recorded from the tip of the trunk circled in (d); g) a typical HRTEM image taken from the tip of the branch. From ref. 149. Copyright © 2004 Wiley-VCH.

parameters $c/a = c/b = 2.2{:}1$; therefore, it is believed that the longer trunk grew in the *c* direction and the two shorter ones in the *a* or *b* direction (Fig. 12c). The selected area electron diffraction patterns (SAED) taken from the branch and main trunk areas marked by the circles in Fig. 12d (Fig. 12 e, f, respectively) are identical, which indicates that they share the same crystal direction along the *c* axis. A typical HRTEM image recorded from the tip of a branch is shown in Fig. 12g. The fringe spacing was about 6.0 Å, which corresponds to the lattice spacing for the (002) faces. This result confirmed the supposition of the growth direction of the dendritic crystal.

The dimensions of such high hierarchical structures finely reflect the outside embodiment of the intrinsic cell structure of stolzite quite well. Further optimization of the growth conditions could make it possible to obtain perfect hierarchical structures.

MWO_4 microspheres (M = Pb, Ca). Nearly monodisperse MWO_4 microspheres (M = Pb, Ca) have been synthesized with the assistance of the surfactants sodium dodecyl benzenesulfonate (SDS) or CTAB *via* the mechanism of oriented attachment.[152] By controlling the solution reaction conditions, nearly monodisperse microspheres of MWO_4 (M = Pb, Ca) composed of subunits with different shapes could be obtained. The diameters of the microspheres were found to be sensitive to the reaction conditions and could be tuned by controlling this. In the formation of $CaWO_4$ subunits the oriented attachment mechanism takes a significant part in the process of self-assembly of quasispherical particles. As shown in Fig. 13a, the subunits of microspheres are in fact nanorods with a diameter of 60 nm and length up to 0.5 μm. The corresponding HRTEM images in Fig. 13b taken from the selected areas marked by the boxes indicate that both the crystal lattices are the same and the fringe spacings along the different directions were determined to be 3.11 Å and 3.70 Å for the (112) and (110) planes respectively. Also in some places of coalescence nanorods display some screw dislocations. The case of $CaWO_4$ further confirmed that at elevated

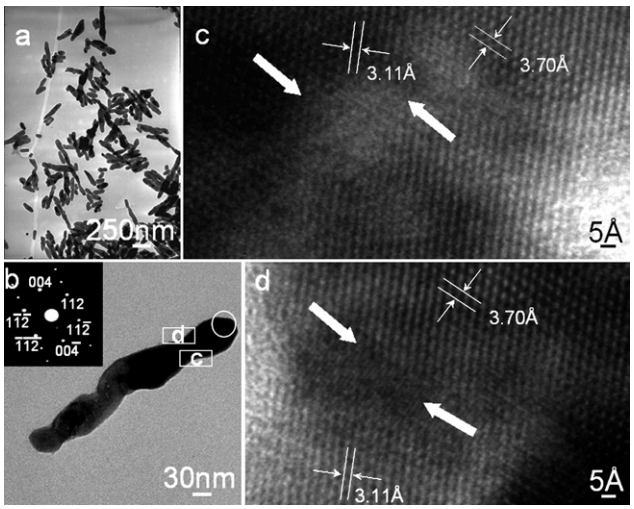

Fig. 13 TEM image and HRTEM images of the subunits collected from broken $CaWO_4$ spheres prepared by aging at 60 °C for 12 h. (a) TEM image of the subunits obtained by ultrasonically treating the spherical microspheres; (b) HRTEM image of a typical nanorod; the inset ED pattern is recorded from the tip of the rod, which is indicated by a circle; (c, d) HRTEM images taken from the areas marked by the boxes in (b). From ref. 152. Copyright © 2007 American Chemical Society.

temperature the Ostwald ripening process dominates the crystal growth process while the oriented attachment process plays a more important role as the temperature decreases due to the lower kinetic energy barrier of this process.

Nowadays, the family of materials obtained by the oriented attachment process in the presence of organic additives is rapidly growing and includes systems as diverse as Co_3O_4,[153] CeO_2,[154] PbS,[155] $NiSe_2$,[156] CoOOH,[157] $CaCO_3$,[66,158] Se,[159] Ag,[160] Pt,[161] Sb_2O_3,[162] etc.

3.2 Oriented attachment growth in the absence of organic additives

In the earlier studies, organic additives had been found to be the key factor for oriented attachment growth, and many surfactants had been used to synthesize anisotropic nanomaterials. However, a report by Weller et al. provided some strong evidence that perfect ZnO nanorods can be conveniently self-assembled from small ZnO quasi-spherical nanoparticles without any organic additives based on the oriented attachment mechanism.[163] In previous studies, the self-assembly of nanoparticles capped by ligands was mainly driven by the interaction of the organic ligands rather than by the interaction of the particle cores as reported by Weller et al. A ZnO sol with an average particle size of approximately 3 nm as shown in Fig. 14a was easily prepared by dropwise adding a 0.03 M solution of KOH (65 mL) in methanol into a solution of zinc acetate dihydrate (0.01 M) in methanol (125 mL) under vigorous stirring at about 60 °C. Refluxing of the concentrated solution leads to the formation of rod-like nanoparticles. Prolonging the heating time mainly leads to an increase of the elongation of the particle along the c axis. After refluxing for one day, single crystalline nanorods with average lengths of 100 nm and widths of approximately 15 nm were formed as shown in Fig. 14b. This is a perfect model case for

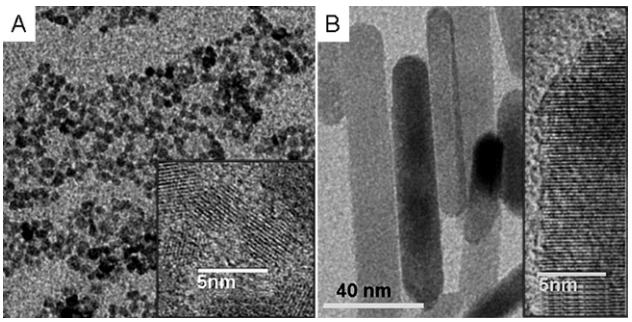

Fig. 14 TEM images of ZnO. (A) starting sol; (B) after one day of reflux of the concentrated sol. The insets show high-resolution TEM images of individual nanoparticles. From ref. 163. Copyright © 2002 Wiley-VCH.

the formation of well-defined one-dimensional nanostructures based on the oriented attachment mechanism without using any ligands or surfactants. There are still an increasing number of examples that are based on oriented attachment and formed in the absence of any organic additives.

$PbCrO_4$. Patil et al. demonstrated the use of liquid–liquid interfaces toward the formation of $PbCrO_4$ nanoparticles and their subsequent time-dependent self-assembly at the air–water interface into nanorods by oriented attachment without the addition of any organic species.[164] Fig.15 shows the evolution process of $PbCrO_4$ nanorods. After aging for 24 h at room temperature, the main products are quasi-rectangular particles with widths ranging from 10 to 30 nm (Fig. 15a). Upon aging the film at room temperature for 48 h, the nanoparticles tend to self-assemble in a linear chain, indicating kinetic governance of the phenomena (Fig. 15b). Under similar conditions, aging up to 120 h revealed the transformation of the linear pearl chain of particle aggregates into single crystalline smooth nanorods (Fig. 15c,d).

TiO_2. Preparation of anatase TiO_2 nanorods from solutions in the absence of any organic surfactants or templates has rarely been reported. Nevertheless, recently, Teng et al.[165–167] point out that hydrothermal treatment of titanate nanotube suspensions under an acidic environment resulted in the formation of single-crystalline anatase nanorods with a specific crystal-elongation direction. The nanotube suspensions were prepared by treatment of TiO_2 in NaOH, followed by mixing with HNO_3 to different pH values. The crystal size of the anatase nanoparticles obtained from the hydrothermal treatment increased with the pH of the suspensions, and nanorods with an aspect ratio up to 6 and a long axis along the anatase [001] were obtained at a pH slightly less than 7. Recently, Banfield et al. pointed out that such oriented attachment processes are usually influenced by the conditions of system, e.g. pH value and temperature.[168]

$ZnWO_4$. Single-crystal $ZnWO_4$ nanorods have been used to direct the self-aggregation of the amorphous nanoparticles and promote the crystallization and transformation process of the amorphous nanoparticles derived from a simple supersaturation precipitation reaction in a nanorod/amorphous nanoparticle coexisting system under refluxing conditions or mild

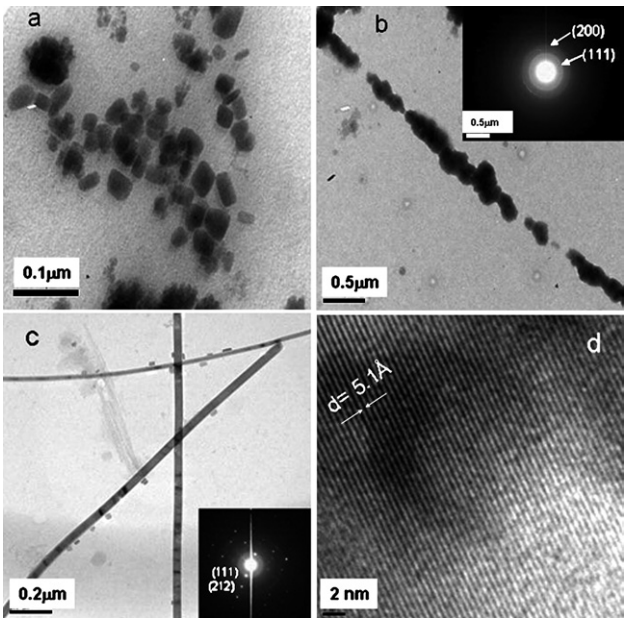

Fig. 15 TEM image of the as-synthesized sample obtained at different aging time at room temperature. (a) Quasi-rectangular nanoparticles after 24 h. (b) Oriented attachment of nanoparticles after 48h. Inset: SAED pattern of the same nanoparticles. (c) Nanorods formed after 120 h. (d) HRTEM image of the nanorods for 120 h. From ref. 164. Copyright © 2008 American Chemical Society.

hydrothermal conditions.[169] In this surfactant/ligand-free system, the obvious nanorod-direct epitaxial aggregation process in the case of $ZnWO_4$ was clearly observed instead of the traditional Ostwald ripening process. The perfect parallel fringes without the misorientations observed by HRTEM (Fig. 16) shows that all small nanoparticles are attached on the nanorods with the same orientation as the uniaxial nanorods. Lattice

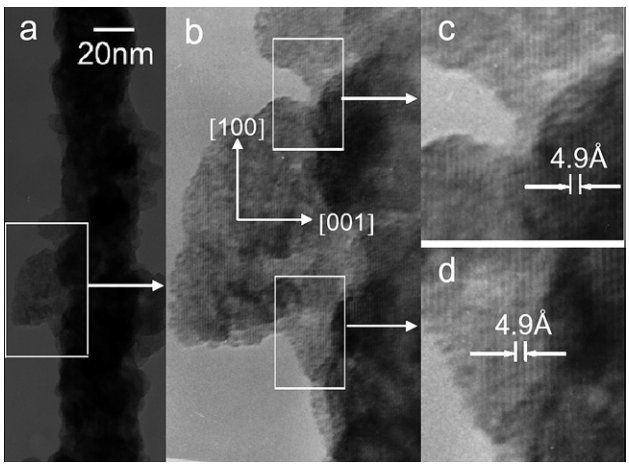

Fig. 16 (a) Typical TEM image of a nanorod with a rough surface obtained by the refluxing a solution containing nanorods and amorphous nanoparticles. (b) High-resolution TEM of the part highlighted in (a). (c and d) The lattice resolved HRTEM images of the areas highlighted in (b), showing that all of the small nanoparticles attached on the nanorods take the same orientation along [100] as the uniaxial of the rods. From ref. 169. Copyright © 2004 American Chemical Society.

resolved HRTEM images in Fig. 16b–d clearly show that all of the outlayers of the rods are composed of tiny nanoparticles with the same orientation along the [100] direction as that observed for the untreated $ZnWO_4$ nanorods. The lattice space was about 4.9 Å, corresponding to the interplanar spacing of (001) planes for $ZnWO_4$. Again, the HRTEM observation from the different parts of the nanorods confirmed that all nanoparticles have the same orientation as the extended nanorods, underlining that the nanorods present in the solution can direct the self-aggregation of the tiny nanoparticles present in the solution. This finding could be universal for various oxide systems or even non-oxide systems. Such spontaneous self-aggregation and crystallization induced by the well-crystallized nanorods could provide a unique route for improving the properties of an anisotropic material due to their rough surface structures made of tiny nanoparticle building blocks and could be used for the formation of more complex crystalline three-dimensional structures in which the branching sites could be added as individual nanoparticles.

CuO. An astonishing example found by Zeng et al. showed that some CuO microspheres synthesized from solution are in fact built from small crystal strips that contain even smaller one-dimensional nanoribbons (Fig. 17).[170] These crystal strips with breadths of about 10–20 nm and lengths not exceeding the strip dimension in [010] (Fig. 17C and 17D), analogous to the "parachutes" in a dandelion, are aligned perpendicularly to the spherical surface, pointing toward a common center. Remarkably, as shown in Fig. 17, the "dandelions" are coreless with a hollow cavity. The thickness of the shell wall is about one-third to one-quarter of the sphere diameter. The feathery shell comprises loosely packed crystal strips, having communicable intercrystal space to its central interior. The nanoribbons are aligned with one another along some main crystallographic axes of CuO *via* an "oriented attachment" process, as elucidated in Fig. 17E which shows that the overall assembly is essentially single crystalline. The dimension of CuO crystal strips has the following hierarchical order [010] > [100] >> [001], while the thickness of the crystal strips in [001] is 20–30 nm.[171] Based on these observation, Zeng et al. have elucidated the two-tiered organizing scheme with multiple-length scales for construction of dandelion-like hollow CuO microspheres in the absence of organic additives: (1) mesoscale formation of rhombic building units from smaller nanoribbons *via* oriented aggregation and (2) macroscopic organization of these units into the CuO microspheres (Fig. 17F).

In addition, Huang et al.[172] have also synthesized two-dimensional (2D) CuO layered oval nanosheets and three-dimensional (3D) nanoellipsoids on a large scale at ~65 °C by a facile template-free method. Shape and dimensionality control of well-defined CuO single crystals could be achieved by simple variations of pH value.

Recently, Wang et al. reported a transition process from one-dimensional $Cu(OH)_2$ nanowires to two-dimensional CuO nanoleaves *via* hierarchical-oriented attachment without use of any surfactant.[173] In this process, polycrystalline $Cu(OH)_2$ nanowires first evolved into single crystalline $Cu(OH)_2$ nanoleaves by an oriented attachment, and then *via* a reconstructive transformation these single crystalline $Cu(OH)_2$ nanoleaves converted into single crystalline CuO nanoleaves, which

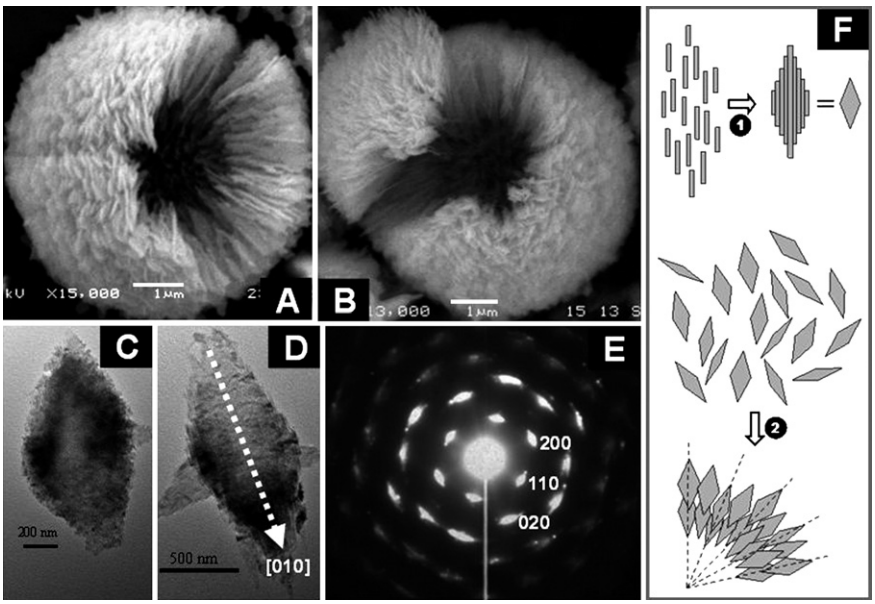

Fig. 17 (A and B) SEM images of two crashed CuO microspheres; (C and D) TEM images of two rhombic CuO crystal strips formed from smaller one-dimensional nanoribbons; (E) SAED pattern ([001] zone) of the crystal strip shown in (D); (F) two-tier organization with multiple-length scales: (1) oriented aggregation of CuO nanoribbons, and (2) concentric alignment of the preformed rhombic building blocks from (1). From ref. 170. Copyright © 2004 American Chemical Society.

consisted of the nucleation of CuO followed by a two-step oriented attachment of the CuO particles. The results demonstrated that in the evolution process of CuO nanostructures, from 0D CuO nanoparticles to 1D CuO nanoribbons and then to 2D CuO nanoleaves, oriented attachment is always playing a significant role, and again the reduction of the overall surface energy by eliminating the surfaces drives the oriented attachment in the whole process.

Gd-doped CeO_2. Very recently, Leite and coworkers[174] have demonstrated that the use of microwave heating during hydrothermal treatment can drastically decrease the treatment time required to obtain gadolinium-doped ceria nanorods and that the oriented attachment is the dominant mechanism responsible for anisotropic growth, implying that it could be possible to introduce the microwave irradiation technique as a parameter to control oriented attachment and anisotropic growth of crystals.

Ag nanodendrites. Wen et al. have also synthesized silver nanodendrites by a simple surfactant-free method using a suspension of zinc microparticles as a heterogeneous reducing agent.[175] Fig. 18A shows a typical dendritic nanostructure at a low magnification. The overall length of the dendrite is about 5 μm, and both the stem and the branches are 20–30 nm in diameter. It is clear that the nanodendrite is highly symmetric, and the angles between the stem and the branches are mostly about 50–60°. The selected area electron diffraction (SAED) pattern (Fig. 18A inset) displays discontinuous concentric rings characteristic of the cubic Ag, indicating that although the whole Ag nanodendrite is not a perfect single crystal, the structure has a certain extent of preferential crystal orientation. The HRTEM image in Fig. 18C from a subbranch (i.e., the third generation) of the Ag nanodendrite shows a robust connection between the

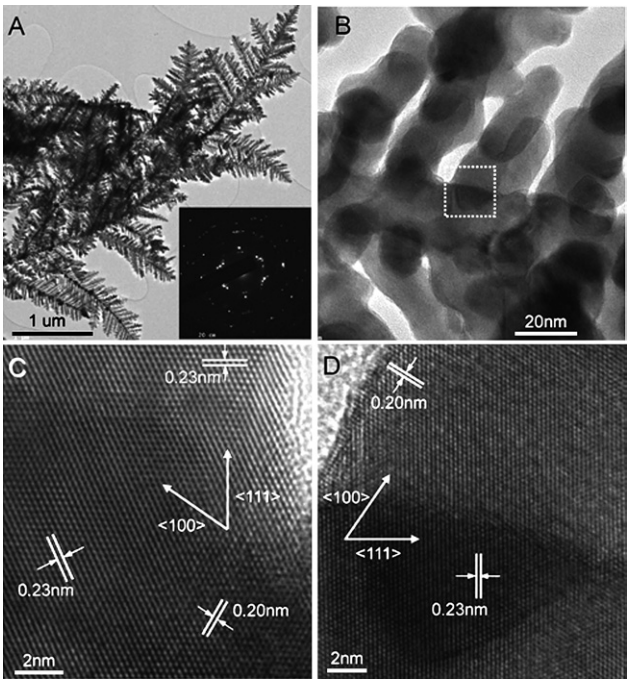

Fig. 18 (A) Low-magnification TEM image of a typical Ag nanodendrite together with an ED pattern (inset); (B) higher magnification TEM image of the Ag nanodendrite; (C) HRTEM image of the Ag nanodendrite in a joint between the stem and a branch; (D) HRTEM image of the Ag nanodendrite in a joint between a branch and a subbranch. From ref. 175. Copyright © 2006 American Chemical Society.

branch and the subbranch. It can be seen that continuous fringes run through both stem and branch (Fig. 18C), indicating that the connection between branch and stem is not simply a physical

contact but rather like an epitaxial growth; both belong to the same crystal system with nearly the same crystal orientation. The fringe spacing perpendicular to the stem measures 0.20 nm, which is very close to the interplanar spacing of (100). Another set of fringes perpendicular to the branch displays a fringe spacing of 0.23 nm, which matches well the interplanar spacing of (111) (Fig. 18C). Fig. 18D shows a HRTEM image of the Ag nanodendrite at another connection site between a branch and one of its subbranches (the part enclosed by the dashed white square in Fig. 18B). The fringes perpendicular to the branch and to the subbranch can be seen clearly with spacings of 0.23 and 0.20 nm, which are assigned to the interplanar spacings of (111) and (100), respectively. According to the analysis above from Fig. 18C,D, it can be concluded that the successive generations from stem, to branch, to subbranch of the nanodendrite grow along <100>, <111> and <100>, respectively.

In addition to the above examples, recently, an increasing number of examples for other inorganic compounds, such as CuO nanorods,[176] anatase TiO_2 nanocrystals,[177] α-Fe_2O_3 nanoparticles,[178] $BiPO_4$ nanorods and BiOCl lamellae,[179] $Cd(OH)_2$ nanodisks,[180] gold sponges,[181] to PbSe/PbS core–shell nanowires and PbS/Au nanowire–nanocrystal heterostructures,[182] have been identified to adopt the oriented attachment as the growth mechanism without additions of any organic additive. These aggregation-based growth mechanisms provide a route for the incorporation of defects, such as edge and screw dislocations, in stress-free and initially defect-free nanocrystalline materials, which could improve the reactivity of the nanocrystalline subunits. Furthermore, this new growth mechanism could offer an additional tool to design functional materials with anisotropic material properties and could be used for the synthesis of more complex crystalline three-dimensional structures in which the branching sites could be added as individual nanoparticles.[163]

3.3 Tailoring of heterostructures

Recently, multifunctional nanomaterials that can respond to multiple external stimuli are attracting more and more attention for their potential applications in novel device.[183] One of these well-known examples is that giant magneto-resistant materials can be used as logic (electronic) and storage (magnetic) components in the same computer chip. Also, incorporation of transition metal oxides on silicon chips is no longer new to the electronic industry with the prospect of ferroelectric oxide being used in nonvolatile ferroelectric random access memory devices.[184] The extension of this approach is integration of magneto-resistive (MR), ferroelectric (FE), and conduction in the same chip providing multifunctionality that ranges from microelectronic to nanospintronics.[185]

Yang and co-workers demonstrated that functional films such as TiO_2 or $Co_{0.05B}Ti_{0.95}O_2$ could be grown epitaxially on SnO_2 to yield functional composite nanotapes, which showed ferromagnetic properties at room temperature.[186] Lieber and co-workers have also synthesized semiconductor core–shell and core–multishell nanowire heterostructures *via* epitaxial growth by modulating the composition of reactant gases in sequential steps.[187] These investigations clearly show the possibility of incorporating multifunctionality into individual 1D nanomaterials, which will find new applications in various fields. There are some reports showing that oriented attachment could be a great tool in fabricating multifunctional nanomaterials.

$ZnWO_4$@MWO_4 (M = Mn, Fe) hybrid nanorods. Our group has reported that $ZnWO_4$ nanorods could direct the formation of heterostructured $ZnWO_4$@MWO_4 (M = Mn, Fe) nanorods by the mechanism of oriented attachment in a ligand-free system.[188] Under mild conditions the crystallization event of MWO_4 could happen on the backbone of $ZnWO_4$ single crystalline nanorods and the shell thickness of MWO_4 could be tuned by changing the molar ratio of raw materials (Scheme 3). Parallel fringes without disorientation observed by HRTEM (Fig. 19) indicated that all the nanoparticles are attached on the nanorods with the same orientation as the uniaxial nanorods, underlying that the $ZnWO_4$ nanorods can direct the self-aggregation of the tiny MWO_4 nanoparticles in the solution. X-Ray photoelectron spectroscopy (XPS) further proves the existence of MWO_4 on the outlayer of nanorods. Photoluminescence (PL) spectra of the as-prepared $ZnWO_4$@$MnWO_4$ and $ZnWO_4$@$FeWO_4$ core–shell nanorods show that they have red shifted from 470 to 475 nm and 470 to 480 nm respectively, which may due to the partial leakage of

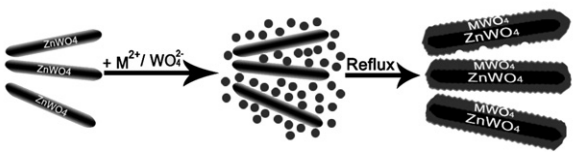

Scheme 3 Schematic illustration of the formation process of the obtained $ZnWO_4$@MWO_4 (M = Mn, Fe) core–shell heteronanostructures. From ref. 188. Copyright © 2007 American Chemical Society.

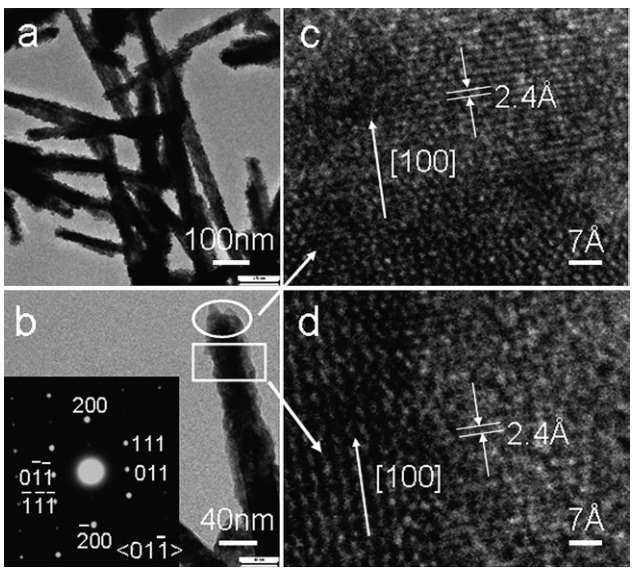

Fig. 19 TEM and HRTEM images of the obtained $ZnWO_4$@$FeWO_4$ core–shell heterostructure. (a,b) TEM images of the product; the inserted ED image in (b) is taken from the tip of the rod, indicated by the white circle. (c,d) HRTEM images taken from the nanorod in (b); their exact positions are marked by the white circle and box, respectively. From ref. 188. Copyright © 2007 American Chemical Society.

excitons into the $MnWO_4$ or $FeWO_4$ matrix. In addition, the phenomenon of antiferromagnetic ordering was observed in these two heterostructures. Thus, this new kind of $ZnWO_4$@MWO_4(M = Mn, Fe) core–shell nanorod with both optical and antiferromagnetic properties may have potential applications.

PbSe/PbS core–shell nanowires. The protection of nanomaterials against oxidation with a thin inorganic epitaxial shell is widely used in highly luminescent II–VI and III–V nanocrystals and nanorods.[189–192] To improve the stability and processability of colloidal PbSe nanowires, Talapin et al.[182] studied the formation of coaxial PbSe/PbS core-shell heterostructures *via* oriented attachment above 180 °C. As shown in Fig. 20a, addition of cubic PbS nanoparticles to a colloidal solution of PbSe nanowires in trioctylamine at 120 °C results in a uniform decoration of the nanowires with PbS nanoparticles. The driving force in this process is the van der Waals interactions between nanowires and nanocrystals. Nanoparticle self-assembly can progress toward the formation of thick layers of nanocubes assembled around PbSe nanowires (Fig. 20b). This self-assembly approach can generate fairly thick PbS "shells" around PbSe nanowires, whereas the shells grown from the molecular precursors are usually only a few nanometers thick. Annealing the nanostructures at 180 °C for 15 min promoted at least partial oriented attachment between nanoparticles and nanowires as show in Fig. 20c. The matching of the lattice fringes in the PbSe nanowire and adjacent PbS nanoparticles as well as the single-crystal like selected area electron diffraction pattern (Fig. 20d) confirm the fusion of PbS nanoparticles with the PbSe nanowire. Decoration of PbSe nanowires with PbS nanoparticles provides a promising architecture for photovoltaic cells with carrier multiplication.

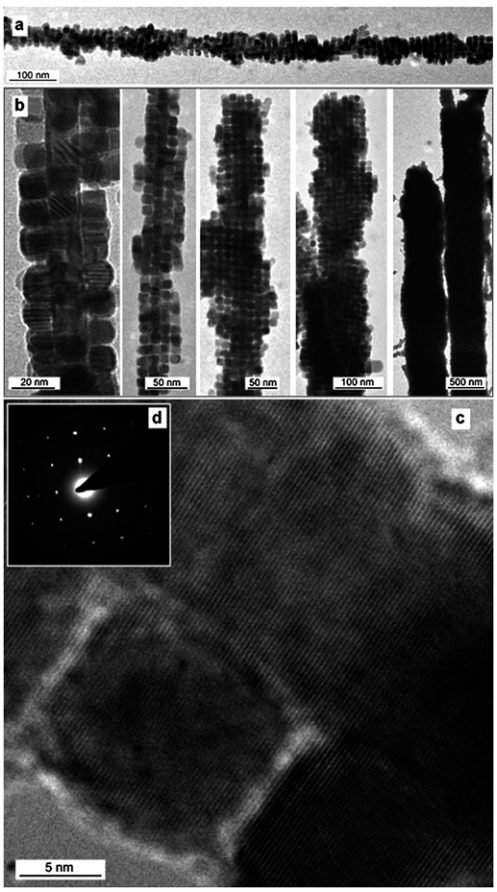

Fig. 20 (a–c) PbSe nanowires with straight, zigzag, and branched morphologies, respectively, used as templates. (d) PbSe-Au nanocomposites synthesized using PbSe nanowires with different morphologies. From ref. 182. Copyright © 2007 American Chemical Society.

There is some other evidence for oriented attachment as a versatile tool in fabricating heterostructures. For example, Ribeiro et al. reported the formation of TiO_2/SnO_2 heterostructures taking advantage of oriented attachment mechanics.[193] Hence, it is expected that this mechanism will open up a new avenue for construction and assembly of multifunctional nanostructures.

4. Summary and outlook

In this paper, the state-of-the-art in the area of the new crystal growth mechanism, so called "oriented attachment", and its potential for application in shape control of a variety of inorganic crystals has been overviewed, including the basic principles and potentials with specific examples, which are very promising for morphology and shape control of various inorganic materials in solution-based systems. The universal applicability of the classical crystallization mechanism was already questioned a few years ago, and the development of alternative crystallization mechanisms is still an important and challenging task.

This oriented attachment mechanism is an important concept involving particle based crystallization pathways. It can yield crystal morphologies that cannot be nucleated *via* a classical ion/molecule based crystallization mechanism. Both the formation and the morphogenesis of single crystals according to this new mechanism apparently contradict the classical textbook knowledge on crystallization, where the growth of shaped crystals is based on the integration of atoms/molecules onto energetically favorable sites on a growing crystal face.[194,195] The adsorption of ions or molecules onto the crystal face is followed by subsequent diffusion across the surface to steps and kink sites[196] and leads to a plane-by-plane growth of a single crystal. The relevant parameters for classical crystallization include molecular solubility (defining the speed of crystallization) and crystal face specific interface tensions defining growth rates, relative exposure and accordingly the morphology of a crystal. However, all these characteristics are certainly not valid for oriented attachment, which is a particle mediated crystallization pathway involving mesoscopic transformation instead.[197]

The emerging oriented attachment process observed under near natural crystallization conditions and spontaneous self-organization of unstabilized nanoparticles could shed new light on understanding of the detailed interaction mechanism between inorganic nanoparticles and their subsequent higher order self-assembly mechanism.[198] In earlier studies, organic additives had been found to be the key factor for oriented attachment growth, and many surfactants had been used to synthesize anisotropic nanomaterials. However, recent progress has provided strong evidence that perfect nanostructures can be conveniently self-assembled from tiny nanoparticles even

without any organic additives based on the oriented attachment mechanism. There are still an increasing number of examples based on oriented attachment and without any organic additives. However, it has to be pointed out that we are still far away from a full understanding of this new growth mechanism, and it is undoubtedly necessary to further investigate this emerging mechanism both experimentally and theoretically.

This new solution route based on the oriented attachment mechanism will certainly open alternative doorways toward rationally designing various kinds of inorganic materials and even multi-component hybrid materials with unique structures, ideal hierarchy, controllable length scale, and multi-functionalities, which will shed new light on their novel applications and fundamental properties.

Acknowledgements

S.-H. Yu acknowledges the funding support from the National Science Foundation of China (NSFC, Grant Nos. 50732006, 20621061, 20671085, 2005CB623601), Anhui Development Fund for Talent Personnel and Anhui Education Committee (2006Z027, ZD2007004-1), the Specialized Research Fund for the Doctoral Program (SRFDP) of Higher Education State Education Ministry, and the Partner-Group of the Chinese Academy of Sciences–the Max Planck Society.

References

1 C. Burda, X. B. Chen, R. Narayanan and M. A. El-Sayed, *Chem. Rev.*, 2005, **105**, 1025.
2 E. R. Leite, Nanocrystals assembled from the bottom up, in: *Encyclopedia of Nnanoscience and Nanotechnology*, ed. H. S. Nalwa, American Scientific Publishers, Stevenson Ranch, CA, 2004, p. 537.
3 A. P. Alivisatos, *J. Phys. Chem.*, 1996, **100**, 13226.
4 H. Boukari, J. S. Lin and M. T. Harris, *J. Colloid Interface Sci.*, 1997, **194**, 311.
5 M. Z. C. Hu, M. T. Harris and C. H. Byers, *J. Colloid Interface Sci.*, 1998, **198**, 87.
6 X. G. Peng, J. Wickham and A. P. Alivisatos, *J. Am. Chem. Soc.*, 1998, **120**, 5343.
7 X. G. Peng, L. Manna, W. D. Yang, J. Wickham, E. Scher, A. Kadavanich and A. P. Alivisatos, *Nature*, 2000, **404**, 59.
8 T. Hyeon, S. S. Lee, J. Park, Y. Chung and H. B. Na, *J. Am. Chem. Soc.*, 2001, **123**, 12798.
9 V. F. Puntes, K. M. Krishnan and A. P. Alivisatos, *Science*, 2001, **291**, 2115.
10 T. Hyeon, Y. Chung, J. Park, S. S. Lee, Y. W. Kim and B. H. Park, *J. Phys. Chem. B*, 2002, **106**, 6831.
11 V. R. Calderone, A. Testino, M. T. Buscaglia, M. Bassoli, C. Bottino, M. Viviani, V. Buscaglia and P. Nanni, *Chem. Mater.*, 2006, **18**, 1627.
12 Z. Y. Tang, N. A. Kotov and M. Giersig, *Science*, 2002, **297**, 237.
13 Y. Volkov, S. Mitchell, N. Gaponik, Y. P. Rakovich, J. F. Donegan, D. Kelleher and A. L. Rogach, *ChemPhysChem.*, 2004, **5**, 1600.
14 J. Polleux, N. Pinna, M. Antonietti and M. Niederberger, *Adv. Mater.*, 2004, **16**, 436.
15 Y. W. Jun, M. F. Casula, J. H. Sim, S. Y. Kim, J. Cheon and A. P. Alivisatos, *J. Am. Chem. Soc.*, 2003, **125**, 15981.
16 B. Cheng, J. M. Russel, W. Shi, L. Zhang and E. T. Samulski, *J. Am. Chem. Soc.*, 2004, **126**, 5972.
17 L. Vayssieres and M. Graetzel, *Angew. Chem. Int. Ed.*, 2004, **43**, 3666.
18 I. I. Naumov, L. Bellaiche and H. X. Fu, *Nature*, 2004, **432**, 737.
19 Y. Xia, P. Yang, Y. Sun, Y. Wu, B. Mayers, B. Gates, Y. Yin, F. Kim and H. Yan, *Adv. Mater.*, 2003, **15**, 353.
20 R. J. Davey, *Nature*, 2004, **428**, 374.
21 W. F. Ostwald, *Phys. Chem.*, 1897, **22**, 289.
22 I. M. Lifshitz and V. V. Slyozov, *Phys. Chem. Solids*, 1961, **22**, 35.
23 C. Wagner, *Thoerie der altering von neiderschlagen durch umlosen. Z Elektrochem.*, 1961, **65**, 581.
24 H. Grätz, *Scrip. Mater.*, 1997, **37**, 9.
25 S. A. Kukushkin and A. V. Osipov, *J. Exp. Theor. Phys.*, 1998, **86**, 1201.
26 Z. S. Hu, G. Oskam, R. L. Penn, N. Pesika and P. C. Searson, *J. Phys. Chem. B.*, 2003, **107**, 3124.
27 G. Oskam, Z. S. Hu, R. L. Penn, N. Pesika and P. C. Searson, *Phys. Rev. E.*, 2002, **66**, 011403.
28 G. Oskam, A. Nellore, R. L. Penn and P. C. Searson, *J. Phys. Chem. B.*, 2003, **107**, 1734.
29 P. Jensen, *Rev. Mod. Phys.*, 1999, **71**, 1695.
30 R. L. Penn and J. F. Banfield, *Am. Mineral.*, 1998, **83**, 1077.
31 R. L. Penn and J. F. Banfield, *Science*, 1998, **281**, 969.
32 R. L. Penn and J. F. Banfield, *Geochim. Cosmochim. Acta.*, 1999, **63**, 1549.
33 F. Banfield, S. A. Welch, H. Zhang, T. T. Ebert and R. L. Penn, *Science*, 2000, **289**, 751.
34 R. L. Penn, G. Oskam, T. J. Strathmann, P. C. Searson, A. T. Stone and D. R. Veblen, *J. Phys. Chem. B*, 2001, **105**, 2177.
35 A. Navrostsky, *Proc. Natl. Acad. Sci.*, 2004, **101**, 12096.
36 E. J. H. Lee, C. Ribeiro, E. Longo and E. R. Leite, *J. Phys. Chem. B*, 2084, **2005**, 109.
37 J. K. Bailey, C. J. Brinker and M. L. Mecartney, *J. Colloid Interface. Sci.*, 1993, **157**, 1.
38 M. Ocana, M. P. Morales and C. J. Serna, *J. Colloid Interface Sci.*, 1995, **171**, 85.
39 Y. F. Zhu, W. R. Zhao, H. R. Chen and J. L. Shi, *J. Phys. Chem. C*, 2007, **111**, 5281.
40 V. Privman, D. V. Goia, J. Park and E. Matijevic, *J. Colloid Interface Sci.*, 1999, **213**, 36.
41 K. Onuma and A. Ito, *Chem. Mater.*, 1998, **10**, 3346.
42 K. S. Cho, D. V. Talapin, W. Gaschler and C. B. Murray, *J. Am. Chem. Soc.*, 2005, **127**, 7140.
43 E. R. Leite, T. R. Giraldi, F. M. Pontes, E. Longo, A. Beltran and J. Andres, *Appl. Phys. Lett.*, 2003, **83**, 1566.
44 M. Adachi, Y. Murata, J. Takao, J. Jiu, M. Sakamoto and F. Wang, *J. Am. Chem. Soc.*, 2004, **126**, 14943.
45 A. Chemseddine and T. Moritz, *Eur. J. Inorg. Chem.*, 1999, 235.
46 F. Huang, H. Z. Zhang and J. F. Banfield, *Nano. Lett.*, 2003, **3**, 373.
47 J. H. Yu, J. Joo, H. M. Park, S. I. Baik, Y. W. Kim, S. C. Kim and T. Hyeon, *J. Am. Chem. Soc.*, 2005, **127**, 5662.
48 A. P. Alivisatos, *Science*, 2000, **289**, 736.
49 J. A. Dirksen and T. A. Ring, *Chem. Eng. Sci.*, 1991, **46**, 2389.
50 C. B. Murray, C. R. Kagan and M. G. Bawendi, *Annu. Rev. Mater. Sci.*, 2000, **30**, 545.
51 B. R. Pamplin. *Crystal Growth*. Pergamon Press: New York, 1975.
52 Y. Jiang, in: *Handbook of nanophase and nanostructured materials*, eds. Z. L. Wang, Y. Liu and Z. Zhang, Kluwer Academic/Plenum Publishers and Tsinghua University Press, 2003, p. 244.
53 I. V. Markov, *Crystal growth for beginners: fundamentals of nucleation, crystal growth and epitaxy*, World Scientific Publishing Co. Pte. Ltd, Singapore, 2003.
54 G. Cao, Nanostructures & Nanomaterials: Synthesis, Properties, & Applications. Imperial College Press, London, 2004.
55 J. D. Yoreo and T. Land, *Sci. Tech. Rev.*, 1996, **9**, 12.
56 H. Cölfen and S. Mann, *Angew. Chem. Int. Ed.*, 2003, **42**, 2350.
57 S. Wohlrab, N. Pinna, M. Antonietti and H. Cölfen, *Chem. Eur. J.*, 2005, **11**, 2903.
58 H. Cölfen and M. Antonietti, *Angew. Chem. Int. Ed.*, 2005, **44**, 5576.
59 A. N. Kulak, P. Iddon, Y. T. Li, S. P. Armes, H. Cölfen, O. Paris, R. M. Wilson and F. C. Meldrum, *J. Am. Chem. Soc.*, 2007, **129**, 3729.
60 D. Schwahn, Y. R. Ma and H. Cölfen, *J. Phys. Chem. C.*, 2007, **111**, 3224.
61 X. Y. Chen, M. H. Qiao, S. H. Xie, K. N. Fan, W. Z. Zhou and H. Y. He, *J. Am. Chem. Soc.*, 2007, **129**, 13305.
62 T. Vossmeyer, G. Reck, L. Katsikas, E. T. K. Haupt, B. Schulz and H. Weller, *Science*, 1995, **267**, 1476.
63 O. Pujol, P. Bowen, P. A. Stadelmann and H. Hofmann, *J. Phys. Chem. B.*, 2004, **108**, 13128.
64 X. H. Guo and S. H. Yu, *Cryst. Growth. Des.*, 2007, **7**, 354.
65 X. H. Guo, A. W. Xu and S. H. Yu, *Cryst. Growth. Des.*, 2007, **7**, 354.

66 A. W. Xu, M. Antonietti, H. Cölfen and Y. P. Fang, *Adv. Funct. Mater.*, 2006, **16**, 903.
67 M. G. Page and H. Cölfen, *Cryst. Growth. Des.*, 2006, **6**, 1915.
68 T. X. Wang, M. Antonietti and H. Cölfen, *Chem. Eur. J.*, 2006, **12**, 5722.
69 J. Zhan, H. P. Lin and C. Y. Mou, *Adv. Mater.*, 2003, **15**, 621.
70 O. Grassmann, R. B. Neder, A. Putnis and P. Löbmann, *Am. Mineral.*, 2003, **88**, 647.
71 S. H. Yu and H. Cölfen, *J. Mater. Chem.*, 2004, **14**, 2124.
72 O. Grassmann and P. Löbmann, *Chem. Eur. J.*, 2003, **9**, 1310.
73 S. H. Yu, H. Cölfen, K. Tauer and M. Antonietti, *Nat. Mater.*, 2005, **4**, 51.
74 Y. R. Ma, H. Cölfen and M. Antonietti, *J. Phys. Chem. B.*, 2006, **110**, 10822.
75 E. V. Shevchenko, D. V. Talapin, A. L. Rogach, A. Kornowski, M. Hasse and H. Weller, *J. Am. Chem. Soc.*, 2002, **124**, 11480.
76 K. X. Yao and H. C. Zeng, *J. Phys. Chem. C.*, 2007, **111**, 13301.
77 J. X. Fang, X. N. Ma, H. H. Cai, X. P. Song and B. J. Ding, *Nanotechnology*, 2006, **17**, 5841.
78 J. X. Fang, B. J. Ding and X. P. Song, *Appl. Phys. Lett.*, 2007, **91**, 083108.
79 J. P. Ge, Y. X. Hu, M. Biazini, W. P. Beyemann and Y. D. Yin, *Angew. Chem. Int. Ed.*, 2007, **46**, 4342.
80 E. Beniash, J. Aizenberg, L. Addadi and S. Weiner, *Proc. R. Soc. London, Ser. B*, 1997, **264**, 461.
81 E. Beniash, L. Addadi and S. Weiner, *J. Struct. Biol.*, 1999, **125**, 50.
82 L. Addadi, S. Raz and S. Weiner, *Adv. Mater.*, 2003, **15**, 959.
83 S. Raz, P. C. Hamilton, F. H. Wilt, S. Weiner and L. Addadi, *Adv. Funct. Mater.*, 2003, **13**, 480.
84 J. Aizenberg, G. Lambert, S. Weiner and L. Addadi, *J. Am. Chem. Soc.*, 2002, **124**, 32.
85 Y. Politi, T. Arad, E. Klein, S. Weiner and L. Addadi, *Science*, 2004, **306**, 1161.
86 S. Weiner, I. Sagi and L. Addadi, *Science*, 2005, **309**, 1027.
87 Y. Oaki and H. Imai, *Small*, 2006, **2**, 66.
88 M. Rousseau, E. Lopez, P. Stempfle, M. Brendle, L. Franke, A. Guette, R. Naslain and X. Bourrat, *Biomaterials*, 2005, **26**, 6254.
89 Y. Oaki and H. Imai, *Angew. Chem. Int. Ed.*, 2005, **44**, 6571.
90 M. Antonietti, M. Breulmann, C. G. Götner, H. Cölfen, K. K. W. Wong, D. Walsh and S. Mann, *Chem. Eur. J.*, 1998, **4**, 2493.
91 L. M. Qi, H. Cölfen, M. Antonietti, M. Li, J. D. Hopwood, A. J. Ashley and S. Mann, *Chem. Eur. J.*, 2001, **7**, 3526.
92 S. H. Yu, H. Cölfen and M. Antonietti, *Chem. Eur. J.*, 2002, **8**, 2937.
93 S. H. Yu, M. Antonietti, H. Cölfen and J. Hartmann, *Nano Lett.*, 2003, **3**, 379.
94 H. Cőlfen, in: *Biomimeralization: from paleontology to materials science*, eds. J. L. Arias and M. S. Fernandez, Editorial Universitaria, Universidad de Chile, Santiago, Chile, 2006.
95 E. Matijević, *Chem. Mater.*, 1993, **5**, 412.
96 E. Matijević, *Curr. Opin. Colloid Interface Sci.*, 1996, **1**, 176.
97 T. Sugimoto, *Adv. Colloid Interface Sci.*, 1987, **28**, 65.
98 J. W. Mullin, in: *Crystallization* (3rd Edition), Butterworth-Heinemann, Stoneham, MA, 1997.
99 H. L. Zhu and R. S. Averback, *Philos. Mag. Lett.*, 1996, **73**, 27.
100 M. Yeadon, M. Ghaly, J. C. Yang, R. S. Averback and J. M. Gibson, *Appl. Phys. Lett.*, 1998, **73**, 3208.
101 R. L. Penn, *J. Phys. Chem. B*, 2004, **108**, 12707.
102 C. Ribeiro, E. J. H. Lee, E. Longo and E. R. Leite, *ChemPhysChem*, 2006, **7**, 664.
103 T. O. Drews, M. A. Katsoulakis and M. Tsapatsis, *J. Phys. Chem. B*, 2005, **109**, 23879.
104 H. G. Yang and H. C. Zeng, *Angew. Chem. Int. Ed.*, 2004, **43**, 5930.
105 H. C. Zeng, *J. Mater. Chem.*, 2006, **16**, 649.
106 J. A. Venables, in: *Introduction to surface and thin film processes*, Cambridge University Press, Cambridge, 2000.
107 H. E. Buckley. *Crystal growth.*, 1951.
108 I. J. W. Mullin. *Crystallization*. Butterworths, London, 1971.
109 A. A. Chernov, *J. Cryst.Growth.*, 1974, **24/25**, 11.
110 T. Kudora, T. Irisawa and A. Ookawa, *J. Cryst. Growth.*, 1977, **42**, 41.
111 W. F. Berg, *Proc. R. Soc. London Ser. A.*, 1938, **164**, 79.
112 C. W. Bunn, *Discuss Faraday Soc.*, 1949, **5**, 132.
113 S. H. Yu, *Top Curr. Chem.*, 2007, **271**, 79.
114 Z. L. Wang, *J. Phys. Chem. B*, 2000, **104**, 1153.
115 H. Cölfen, *Top Curr. Chem.*, 2007, **271**, 1.
116 G. Garnweitner and M. Niederberger, *J. Mater. Chem.*, 2008, **18**, 1171.
117 S. H. Yu and S. F. Chen, *Current Nanosci.*, 2006, **2**, 81.
118 A. C. Curtis, D. G. Duff, P. P. Edwards, D. A. Jefferson, B. F. G. Johnson, A. I. Kirkland and A. S. Wallace, *Angew. Chem. Int. Ed.*, 1988, **27**, 1530.
119 T. S. Ahmadi, Z. L. Wang, T. C. Green, A. Henglein and M. A. El-Sayed, *Science*, 1996, **272**, 1924.
120 J. S. Bradley, B. Tesche, W. Busser, M. Maase and M. T. Reetz, *J. Am. Chem. Soc.*, 2000, **122**, 4631.
121 Y. Sun and Y. Xia, *Science*, 2002, **298**, 2176.
122 N. K. Raman, M. T. Anderson and C. J. Brinker, *Chem. Mater.*, 1996, **8**, 1682.
123 S. Mann, S. L. Burkett, S. A. Davis, C. E. Fowler, N. H. Mendelson, S. D. Sims, D. Walsh and N. T. Whilton, *Chem. Mater.*, 1997, **9**, 2300.
124 L. A. Estroff and A. D. Hamilton, *Chem. Mater.*, 2001, **13**, 3227.
125 S. A. Davis, M. Breulmann, K. H. Rhodes, B. Zhang and S. Mann, *Chem. Mater.*, 2001, **13**, 3218.
126 R. A. Caruso and M. Antonietti, *Chem. Mater.*, 2001, **13**, 3272.
127 K. J. C. van Bommel, A. Friggeri and S. Shinkai, *Angew. Chem. Int. Ed.*, 2003, **42**, 980.
128 J. Polleux, N. Pinna, M. Antonietti, C. Hess, U. Wild, R. Schlögl and M. Niederberger, *Chem. Eur. J.*, 2005, **11**, 3541.
129 M. Niederberger, M. H. Bartl and G. D. Stucky, *J. Am. Chem. Soc.*, 2002, **124**, 13642.
130 M. Niederberger, G. Garnweitner, F. Krumeich, R. Nesper, H. Cölfen and M. Antonietti, *Chem. Mater.*, 2004, **16**, 1202.
131 M. Niederberger, M. H. Bartl and G. D. Stucky, *Chem. Mater.*, 2002, **14**, 4364.
132 L. Wang, X. Guan, H. Yin, J. Moradian-Oldak and G. H. Nancollas, *J. Phys. Chem. C*, 2008, **112**, 5892.
133 N. Pradhan, H. Xu and X. G. Peng, *Nano. Lett.*, 2006, **6**, 720.
134 L. Manna, E. C. Scher and A. P. Alivisatos, *J. Am. Chem. Soc.*, 2000, **122**, 12700.
135 Z. A. Peng and X. Peng, *J. Am. Chem. Soc.*, 2001, **123**, 1389.
136 P. D. Cozzoli, L. Manna, M. L. Curri, S. Kudera, C. Giannini, M. Striccoli and A. Agostiano, *Chem. Mater.*, 2005, **17**, 1296.
137 J. W. Grebinski, K. L. Hull, J. Zhang, T. H. Kosel and M. Kuno, *Chem. Mater.*, 2004, **16**, 5260.
138 C. Ma and Z. L. Wang, *Adv. Mater.*, 2005, **17**, 2635.
139 A. Halder and N. Ravishankar, *Adv. Mater.*, 2007, **19**, 1854.
140 D. Zitoun, N. Pinna, N. Frolet and C. Belin, *J. Am. Chem. Soc.*, 2005, **127**, 15034.
141 Z. Tang and N. A. Kotov, *Adv. Mater.*, 2005, **17**, 951.
142 Z. P. Zhang, H. Sun, X. Shao, D. Li, H. Yu and M. Han, *Adv. Mater.*, 2005, **17**, 42.
143 M. Li, H. Schnablegger and S. Mann, *Nature*, 1999, **402**, 393.
144 M. Li and S. Mann, *Langmuir*, 2000, **16**, 7088.
145 L. M. Qi, H. Cölfen and M. Antonietti, *Angew. Chem. Int. Ed.*, 2000, **39**, 604.
146 L. M. Qi, H. Cölfen and M. Antonietti, *Chem. Mater.*, 2000, **12**, 2392.
147 M. Li, S. Mann and H. Cölfen, *J. Mater. Chem.*, 2004, **14**, 2269.
148 S. H. Yu, H. Cölfen and M. Antonietti, *Adv. Mater.*, 2003, **15**, 133.
149 B. Liu, S. H. Yu, L. Li, Q. Zhang, F. Zhang and K. Jiang, *Angew. Chem. Int. Ed.*, 2004, **43**, 4745.
150 D. Kuang, A. Xu, Y. Fang, H. Liu, C. Frommen and D. Fenske, *Adv. Mater.*, 2003, **15**, 1747.
151 Y. Ma, L. Qi, J. Ma and H. Cheng, *Cryst. Growth. Des.*, 2004, **4**, 351.
152 Q. Zhang, W. T. Yao, X. Y. Chen, L. W. Zhu, Y. B. Fu, G. B. Zhang, L. S. Sheng and S. H. Yu, *Cryst. Growth. Des.*, 2007, **7**, 1423.
153 T. He, D. Chen and X. Jiao, *Chem. Mater.*, 2004, **16**, 737.
154 R. Si, Y. W. Zhang, L. P. You and C. H. Yan, *J. Phys. Chem. B*, 2006, **110**, 5994.
155 F. Zuo, S. Yan, B. Zhang, Y. Zhao and Y. Xie, *J. Phys. Chem. C*, 2008, **112**, 2831.
156 W. M. Du, X. F. Qian, X. S. Niu and Q. Gong, *Cryst. Growth. Des.*, 2007, **7**, 2733.
157 R. L. Penn, A. T. Stone and D. R. Veblen, *J. Phys. Chem. B*, 2001, **105**, 4690.
158 N. Gehrke, H. Cölfen, N. Pinna, M. Antonietti and N. Nassif, *Cryst. Growth. Des.*, 2005, **5**, 1317.

159 J. M. Song, Y. J. Zhan, A. W. Xu and S. H. Yu, *Langmuir*, 2007, **23**, 7321.
160 M. Giersig, I. PastorizaiSantos and L. M. Liz-Marzán, *J. Mater. Chem.*, 2004, **14**, 607.
161 Y. Yamauchi, T. Momma, M. Fuziwara, S. S. Nair, T. Ohsuna, O. Terasaki, T. Osaka and K. Kuroda, *Chem. Mater.*, 2005, **17**, 6342.
162 Z. T. Deng, D. Chen, F. Q. Tang, X. W. Meng, J. Ren and L. Zhang, *J. Phys. Chem. C*, 2007, **14**, 5325.
163 C. Pacholski, A. Kornowski and H. Weller, *Angew. Chem. Int. Ed.*, 2002, **41**, 1188.
164 R. R. Hawaldar, S. D. Sathaye, A. Harle, R. S. Gholap and K. R. Patil, *J. Phys. Chem. C*, 2008, **112**, 7557.
165 C. C. Tsai and H. Teng, *Chem. Mater.*, 2004, **16**, 4352.
166 C. C. Tsai and H. Teng, *Chem. Mater.*, 2006, **18**, 367.
167 J. N. Nian and H. Teng, *J. Phys. Chem. B*, 2006, **110**, 4193.
168 M. P. Finnegan, H. Zhang and J. F. Banfield, *Chem. Mater.*, 2008, **20**, 3443.
169 B. Liu, S. H. Yu, L. Li, F. Zhang, Q. Zhang, M. Yoshimura and P. Shen, *J. Phys. Chem.*, 2004, **108**, 2788.
170 B. Liu and H. C. Zeng, *J. Am. Chem. Soc.*, 2004, **126**, 8124.
171 Y. Chang and H. C. Zeng, *Cryst. Growth. Des.*, 2004, **4**, 397.
172 J. Liu, X. Huang, Y. Li, K. M. Sulieman, X. He and F. Sun, *Cryst. Growth. Des.*, 2006, **6**, 1690.
173 H. L. Xu, W. Z. Wang, W. Zhu, L. Zhou and M. L. Ruan, *Cryst. Growth. Des.*, 2007, **7**, 2720.
174 M. Godinho, C. Ribeiro, E. Longo and E. R. Leite, *Cryst. Growth. Des.*, 2008, **8**, 384.
175 X. Wen, Y. T. Xie, M. W. C. Mak, K. Y. Cheung, X. Y. Li, R. Renneberg and S. Yang, *Langmuir*, 2006, **22**, 4836.
176 W. T. Yao, S. H. Yu, Y. Zhou, J. Jiang, Q. S. Wu, L. Zhang and J. Jiang, *J. Phys. Chem. B*, 2005, **109**, 14011.
177 C. H. Cho, M. H. Han, D. H. Kim and D. K. Kim, *Mater. Chem. Phys.*, 2005, **92**, 104.
178 C. Frandsen, C. R. H. Bahl, B. Lebech, K. Lefmann, L. Theil Kuhn, L. Keller, N. H. Andersen, M. V. Zimmermann, E. Johnson, S. N. Klausen and S. Mørup, *Phys. Rev. B*, 2005, **72**, 214406–1.
179 J. Geng, W. H. Hou, Y. N. Lv, J. J. Zhu and H. Y. Chen, *Inorg. Chem.*, 2005, **44**, 8503.
180 W. Shi, C. Wang, H. Wang and H. Zhang, *Cryst. Growth. Des.*, 2006, **6**, 915.
181 Y. X. Zhang and H. C. Zeng, *J. Phys. Chem. C*, 2007, **111**, 6970.
182 D. V. Talapin, H. Yu, E. V. Shevchenko, A. Lobo and C. B. Murray, *J. Phys. Chem. C*, 2007, **111**, 14049.
183 L. Wang, J. Bai, Y. Li and Y. Huang, *Angew. Chem. Int. Ed.*, 2008, **47**, 2439.
184 V. L. Mathe, *J. Magn. Magn. Mater.*, 2003, **263**, 344.
185 S. Jin, T. H. Tiefel, M. McCormack, R. A. Fastnacht, R. Ramesh and L. H. Chen, *Sicence*, 1994, **264**, 413.
186 R. H. He, M. Law, R. Fan, F. Kim and P. D. Yang, *Nano Lett.*, 2002, **2**, 1109.
187 L. J. Lauhon, M. S. Gudiksen, D. Wang and C. M. Lieber, *Nature*, 2002, **420**, 57.
188 Q. Zhang, X. Y. Chen, Y. X. Zhou, G. B. Zhang and S. H. Yu, *J. Phys. Chem. C*, 2007, **111**, 3927.
189 M. A. Hines and P. Guyot-Sionnest, *J. Phys. Chem.*, 1996, **100**, 468.
190 D. V. Talapin, I. Mekis, S. Gotzinger, A. Kornowski, O. Benson and J. Weller, *J. Phys. Chem. B*, 2004, **108**, 8826.
191 Y. W. Cao and U. Banin, *J. Am. Chem. Soc.*, 2000, **12**, 9692.
192 L. Manna, E. C. Scher, L. S. Li and A. P. Alivisatos, *J. Am. Chem. Soc.*, 2002, **124**, 7136.
193 C. Ribeiro, E. Longo and E. R. Leite, *Appl. Phys. Lett.*, 2007, **91**, 103105.
194 W. Kossel. *Mathematisch-Physische Klasse*, 1927, pp. 135–143.
195 I. N. Stranski, *Z. Phys. Chem.*, 1928, **136**, 259.
196 W. K. Burton, N. Cabrera and F. C. Frank, *Philos. Trans. R. Soc. London Ser. A*, 1951, **243**, 299.
197 M. Niederberger and H. Cölfen, *Phys. Chem. Chem. Phys.*, 2006, **8**, 3271.
198 S. H. Yu and H. Cölfen, "Nature-inspired Nanoparticle Superstructures", in: *Nanoparticle Superstructures*, CRC Press, Taylor & Francis Group, FL, ed. N. N. Kotov, 2005, Chapter 11, pp. 269–338.